Energy Conversion and Management 261 (2022) 115666

Contents lists available at ScienceDirect

Energy Conversion and Management

journal homepage: www.elsevier.com/locate/enconman

Optimal reconfiguration of PV array based on digital image encryption algorithm: A comprehensive simulation and experimental investigation

Rayappa David Amar Raj *, Kanasottu Anil Naik

Department of Electrical Engineering, National Institute of Technology, Warangal, Telangana, India

ARTICLE INFO

Keywords:
Arnold's Cat Map
Mismatch
Power peaks
Reconfiguration
Shade dispersion

ABSTRACT

Harvesting the optimal output from partially shaded PV arrays is a crucial issue. To address this, various reconfiguration techniques are reported in the literature. However, most of these techniques inherit numerous drawbacks such as compatibility issues, ineffective shade dispersal, numerous power peaks, inconsistent performance, increased mismatch, etc. Therefore, a novel reconfiguration approach based on Arnold's Cat Map which is widely employed in image encryption is proposed in this work to overcome all the aforementioned issues. The proposed approach is tested for various symmetrical 9 × 9, 7 × 7, 6 × 6, 5 × 5, 4 × 4, and unsymmetrical 3 × 5, 4 × 3, 5 × 9, and 6 × 20 PV arrays under 100 shading cases. The performance of the proposed technique is compared with the 41 existing reconfiguration techniques for various array sizes. The proposed technique is experimentally validated in both indoor laboratory and outdoor environments for 4 × 4 and 3 × 5 PV arrays under distinct shading conditions. Further, to confirm the effectiveness and consistency of the proposed technique over the existing ones statistically, a Non-parametric Wilcoxon Signed-Rank test with a significant difference of 0.05 is considered for evaluation. The proposed technique yields the maximum enhancement in output by 30.81%, 36.36%, 38.15%, 33.77%, 16.62%, 21.8%, 18.42%, and 16.79% for 9 × 9, 7 × 7, 6 × 6, 5 × 5, 4 × 4, 4 × 3, 5 × 9, and 6 × 20 PV arrays respectively. From the comprehensive analysis, it is remarked that the lowest mismatch is obtained by the proposed encryption based-technique under all shading conditions.

1. Introduction

The steadfast augmentation of solar energy resources towards electricity production has been a great boon to the world [1]. The numerous advantages associated with PV energy resources transcend other resources [2]. The PV array constitutes several PV panels configured in series and parallel to obtain the rated output [3]. Some of the notable conventional array configurations are Series-Parallel, Bridge-Link, Honey-Comb, and Total-Cross-Tied (TCT). Nevertheless, the PV array performance is greatly limited by frequently occurring partial shading phenomena caused by buildings, trees, clouds, soiling, bird-droppings etc. During shading, there exists a significant mismatch between the row-currents of an array leading to mismatch losses and multiple power peaks (MPPs) in array characteristics. MPPT controllers are employed to track global maximum power (GMP) under shading [4]. These peaks mislead the MPPT controllers in tracking of GMP resulting in increased power loss. The mismatch losses are highly dependent on the type of array configuration and shading pattern [5]. These losses can be highly alleviated by reducing the mismatch between rows through effective shade dispersal. However, all the conventional configurations have zero shade distribution ability resulting in huge losses. To maximize the array output beyond what is attainable solely by employing MPPT controllers, the PV array reconfiguration strategies are recommended [6]. Further, unlike conventional configurations [7], these reconfiguration strategies have shade dispersion ability leading to uniform row currents in an array and smooth characteristics.

These strategies are categorized as static and dynamic strategies. Static reconfiguration is a one-time reconfiguration based on the physical relocation of panels without altering electrical connections. In dynamic reconfiguration, the panels are dynamically reconfigured by changing the electrical circuitry without involving panel relocation. Table 1 gives the detailed comparative literature review of static and dynamic reconfiguration techniques reported in the literature. The notable remarks and shortcomings/limitations of all the techniques are mentioned alongside. Dynamic reconfiguration mainly includes electrical array reconfiguration (EAR) [8–10], artificial intelligence (AI) [11–12], Metaheuristic-based [13–18] strategies which effectively

* Corresponding author.
E-mail address: dtcdavid2k15@gmail.com (R.D.A. Raj).

https://doi.org/10.1016/j.enconman.2022.115666
Received 19 February 2022; Received in revised form 4 April 2022; Accepted 20 April 2022
Available online 29 April 2022

Nomenclature

Abbreviations

ACM	Arnold's cat map
ADV	Advanced-sudoku
AI	Artificial intelligence
AS	Arrow-sudoku
CB	Chaotic-baker
CM	Chaos map
CS	Canonical-sudoku
DACM	Discrete Arnold's cat map
DS	Dominance-square
DTCT	Diagonal-TCT
EAR	Electrical array reconfiguration
FL	Fuzzy logic
FP	Futoshiki puzzle
GA	Genetic algorithm
GMP	Global maximum power
HHO	Harris hawk's optimization
HM	Henon map
IS	Improved sudoku
JP	Jigsaw puzzle
KK	Ken-ken
LAS	Latin square
LS	Lo-shu
LSP	L-shaped propagated
MDS	Multi-diagonal sudoku
MMPs	Multiple power peaks
MPPT	Maximum power point tracking
MS	Magic square
MSE	Mean square error
NA	New array reconfig. scheme
NCI	New-column-index
NOS	Non-optimal-sudoku
NSD	Novel-shade-dispersion
NTCT	Novel TCT
OE	Odd-Even
OEP	Odd-Even-Prime
OPS	Optimized sudoku
OS	Optimal sudoku
OTCT	Optimal TCT
PSNR	Peak signal-to-noise ratio
PSO	Particle swarm optimization
RLS	Recursive-least-squares
SD	Sudoku puzzle
SDK	Sudoku
SKP	Skyscraper puzzle
SMT	Shift-modified TCT
SP	Series-parallel
SSIM	Structural similarity index
TCT	Total-cross-tied
TT	Triple-Tied-Cross-Linked

enhance the output under shading. Notwithstanding, they have numerous challenges. EAR and AI-based techniques [8–12] necessitate numerous switches, sensors, switching matrix, relays, controllers, etc. for execution which is not economically and practically feasible. Further, the Metaheuristic-based techniques [13–18] involve complicated algorithms, convergence issues, computational complexity, complex search mechanisms, parameters tuning challenges, etc. Besides, many of these techniques employ a weighted-sum-approach resulting in sub-optimal output if improper weights are selected. Assigning proper weights is also a challenging task. To evade all these serious issues, static reconfiguration techniques are preferred over dynamic ones.

These static techniques [19–46] are grouped as puzzle-based, Shift-based, Indexing-based, Magic-square-based, Analytical, and Image processing-based reconfiguration techniques which don't necessitate any switches, sensors, relays, etc. for operation. Hence, they provide an economical and practically feasible solution for shading-related issues. Nevertheless, as mentioned in Table 1, the majority of the static reconfiguration techniques reported in the literature suffer serious limitations. The application of the puzzle-based techniques [19–26,29,36–37,40–41,44–45] is highly limited as they work on the principle of various logic puzzles whose application is strictly limited to certain array sizes only. Additionally, there exists hundreds of solutions exist for these puzzles. Ascertaining the best puzzle pattern for optimal reconfiguration among all these solution sets is highly challenging and burdensome. The employment of magic-square (MS) techniques [30,35,42] is much narrower as they are suitable only for very limited array sizes. For instance, the Lo-Shu technique [30] applies only for 3×3 and 9×9 grids. Both puzzle-based and MS-based techniques have very limited application for symmetrical $n \times n$ arrays and are not compatible with all unsymmetrical $m \times n$ arrays. The Shift-based techniques [27,33,43] fail to effectively disperse the shade as 34% of the panels of a particular row remain still even after reconfiguration. Besides, the Indexing-based techniques [28] also fail to relocate all the panels of a row. Despite employing this approach, 45% of the panels remain unchanged in a row thereby failing to yield an optimal solution. Moreover, the compatibility of the shift-based and indexing-based techniques have not been verified for the unsymmetrical PV arrays. Further, the analytical strategies [31–32,46], despite being applicable to all array sizes exhibit poor shading dispersal with increased mismatch and numerous MPPs in array characteristics. The recently reported analytical strategies such as OE [31] and OEP [32] exhibit highly inferior performance as (45–50) % of the panels of a particular row remain unchanged. Hence, they are only 50% efficient in dispersing the shade over the array. This is a major drawback. The image processing-based techniques [34,38] are employed recently to mitigate the shading impact and MPPs. However, these techniques, despite being effective compared to the conventional array configurations, exhibit uneven shade dispersion due to their ineffective reconfiguration. Additionally, these techniques are not compatible with unsymmetrical array sizes.

From the comprehensive literature survey (Table 1), the **majorly identified research gaps** and issues that are to be addressed are noted as follows:

- A generalized and universally compatible reconfiguration approach is to be devised that can be scalable for all sizes of symmetrical and unsymmetrical PV arrays.
- Most of the existing techniques, despite being effective in enhancing the GMP to some extent, induce numerous MPPs in the array characteristics. Hence, the burden on MPPT controllers is increased significantly in differentiating the global and local power peaks. So, high-cost, sophisticated and complex controllers are necessitated for tracking GMP.
- As most of the existing static techniques reconfigure the array arbitrarily through some puzzle-based pattern or magic-square-pattern, etc. the shading is not uniformly dispersed, and sometimes even results in significantly less output than it has generated before reconfiguration. So, an intelligent and even shade dispersion can eliminate this drawback.
- The reconfiguration algorithm should be consistently superior, reliable, and effective in dispersing the shade during all types of shading conditions (and not just under some cases).

Table 1
Literature survey of various PV array reconfiguration strategies.

Ref., year	Technique	Type	Array size	Remarks	Limitations/Shortcomings
[8], 2015	Munkres-Algorithm	Dynamic, EAR	3 × 3	Obtained sub optimal array configuration that requires fewer switching operations	Slow convergence, requires huge no. of switches, complex algorithm, practical feasibility issues
[9], 2019	Modified -Circuit	Dynamic, EAR	2 × 2, 2 × 3, 3 × 2	Prototypes of two circuit models (square & rectangle) are modified using switches	Low power enhancement in many shading cases
[10], 2020	Two-Step Approach	Dynamic, EAR	4 × 4	No. of switches necessitated is less mitigating the switching losses	Slow convergence, Effectiveness compared with only conventional TCT
[11], 2016	Fuzzy-Logic (FL)	Dynamic, AI based	3 × 4	Electrical connections are altered, optimal switching matrix is detected by FL output	Employs switching matrix, sensors, switches, micro-controllers, high-cost, practical complexity
[12], 2021	Fuzzy-Logic & Recursive-least-squares (RLS)	Dynamic, AI based	1 × 1, 4 × 4	FL estimates optimized switching configuration, uses RLS for irradiation estimation	Tested under unrealistic shading cases, experimentally verified only for 1 × 1 array, implementation for medium/ large arrays is challenging task
[13], 2015	Genetic Algorithm (GA)	Dynamic, Metaheuristic	9 × 9	Performance is compared with static sudoku technique under 3 distinct shading cases	Employs a weighted sum approach which is a major drawback, determining optimal weights is highly challenging
[14], 2020	Particle Swarm Optimization (PSO)	Dynamic, Metaheuristic	9 × 9	Finds optimal switching matrix based on PSO, Yields better shade dispersal	Algorithm prone to struck in local optimum, complex algorithm and search mechanism, parameters tuning difficulty, premature convergence
[15], 2020	Multi-Objective Grey Wolf Optimization	Dynamic, Metaheuristic	9 × 9	Solved as multi-objective problem maximizing the array power & minimizing the row current error	Huge computations, tested only under square patterned shading cases, slow convergence
[16], 2020	Harris Hawks Optimization (HHO)	Dynamic, Metaheuristic	9 × 9, 6 × 20	Simple and easy to implement, requires a smaller number of control parameters	Algorithm involves several stages, generates numerous MPPs even compared to conventional TCT
[17], 2020	Coyote Optimization Algorithm	Dynamic, Metaheuristic	9 × 9	GMP is enhanced compared to MPA and BOA techniques, reduces mismatch losses	Algorithm is tested only for 9 × 9 PV array, search mechanism is complex
[18], 2021	Democratic Political Algorithm	Dynamic, Metaheuristic	10 × 10,15 × 15, 20 × 20	Yields better output performance compared to many Metaheuristic optimization techniques	Search mechanism is complex, increased computational burden
[19], 2013	Sudoku (SDK)	Static, Number-placement	9 × 9	Panels are physically relocated based on sudoku puzzle pattern without altering electrical circuitry	
[20], 2019	Optimal-Sudoku (OS)	Static, Logic-sequence	9 × 9	Physical relocation based on Optimal-sudoku pattern	Cannot be applicable other than 9n × 9n PV array sizes, Numerous sudoku solutions are possible, hence finding the optimal sudoku-pattern for particular sudoku-variant is impossible, Complexity increases with the array size, Incompatible for unsymmetrical PV arrays, Power enhancement not guaranteed under all shading cases, uneven shade dispersion, First column of array is unchanged in some sudoku-variants
[21], 2019	Improved-Sudoku (IS)	Static, Number-placement	9 × 9	Physical relocation based on Improved-sudoku pattern	
[22], 2021	Advanced-sudoku (ADV)	Static, Puzzle-based	9 × 9	Physical relocation based on advanced-sudoku pattern	
[23], 2021	Canonical-sudoku (CS)	Static, Puzzle-based	9 × 9	Physical relocation based on Canonical-sudoku pattern	
[23], 2021	Multi-diagonal -Sudoku (MDS)	Static, Logic-Puzzle	9 × 9	Physical relocation based on multi-diagonal-sudoku pattern	
[24], 2018	Non-optimal-Sudoku (NOS)	Static, Logic-Puzzle	9 × 9	Physical relocation based on modified-sudoku pattern under mutual shading	
[24,25] 2018	Futoshiki-Puzzle (FP)	Static, Logic-Puzzle	9 × 9, 5 × 5	Shade dispersion by Futoshiki-Puzzle pattern	Not applicable for all n × n and m × n array sizes
[26], 2015	Optimal Sudoku-based (OSB)	Static, Logic-Puzzle	9 × 9	Mitigates mismatch and line losses by optimizing sudoku-pattern	Same limitations as that of sudoku-puzzle
[27], 2017	Shift-modified-TCT (SMT)	Static, Shift-based	9 × 9, 3 × 3, 2 × 2	Alleviates MPPs through shade distribution over entire array	34% panels of a row remain same even after reconfiguration. Limited analysis, Low power enhancement
[28], 2018	New-column-index (NCI)	Static, Index-based	9 × 9	Proposed a One-time fixed interconnection scheme using a column index numbering scheme	Effective shade dispersion is not guaranteed as the reconfigured array obtained by CI scheme doesn't relocate all the elements of a row in PV array.
[29], 2019	Skyscapper-Puzzle (SKP)	Static, Logic-Puzzle	9 × 9, 5 × 5	One-time fixed reconfiguration is done by using the skyscraper puzzle pattern	Exists numerous solution sets for Skyscraper puzzle. Not compatible for all array sizes.
[30], 2020	Lo-shu (LS)	Static, Magic-square	9 × 9	Shade dispersion based on Lo-Shu Magic square technique by one-time fixed reconfiguration	Cannot be employable other than 9 × 9 array size. Not employable for unsymmetrical arrays.
[31], 2020	Odd-Even (OE)	Static, Analytical	7 × 7	One-time configuration based on Odd-Even numbering of panels, compatible with all arrays	Poor shade dispersion capability, exhibits numerous MPPs
[32], 2020	Odd-Even-Prime (OEP)	Static, Analytical	9 × 9	Fixed configuration based on Odd-Even-Prime numbering of panels, applicable for all array sizes	Tested only under square type of shadings, exhibits poor shade dispersion ability and numerous MPPs
[33], 2020	New Array Reconfig. Scheme (NA)	Static, Diagonal-arrangement	9 × 9	Physical relocation of panels in diagonal-manner	Tested under only two shading patterns, Compared only with conventional TCT, Poor shade dispersion
[34], 2021	Chaos Map (CM)	Static, Image processing	7 × 7, 6 × 6	Image processing-based technique applicable to all symmetrical arrays	50% of panels remain unchanged in same row even after reconfiguration, Poor shade dispersal in odd-symmetrical arrays, incompatible with unsymmetrical arrays
[35], 2016	Magic-square (MS)	Static, Magic-square	3 × 3, 6 × 6	Relocation based on Magic-square pattern	Very limited application, incompatible with unsymmetrical arrays

(*continued on next page*)

Table 1 (*continued*)

Ref., year	Technique	Type	Array size	Remarks	Limitations/Shortcomings
[36], 2018	Ken-ken (KK)	Static, logic-Puzzle	6 × 6	Aims to enhance output and mitigate wiring losses	Low power enhancement, not scalable
[36], 2018	Latin-square (LAS)	Static, Puzzle-based	6 × 6		Yields lowest output under diagonal shading, compatibility issues
[37], 2019	Arrow-sudoku (AS)	Static, logic-Puzzle	6 × 6	Analysed under three distinct dynamic continuous shadings	Compared only with conventional configurations, incompatibility issues
[38], 2019	Chaotic-Baker-Map (CB)	Static, Image processing	6 × 6, 4 × 4	Shade dispersion based on concept of image processing	Low power enhancement, effectiveness compared only with conventional configurations, exhibits numerous MPPs
[39], 2021	Triple-Tied-Cross-Linked (TT)	Static, conventional	9 × 9	Mitigates interconnection ties than TCT	Zero shade dispersal, lower output than TCT
[40], 2020	Skyscraper (SKY)	Static, logic-Puzzle	6 × 6	Reduces wiring losses	low power enhancement, compared only with AS, compatibility issues
[41], 2018	Dominance-square (DS)	Static, Number placement	5 × 5	Reconfigured based on dominance square puzzle pattern	Cannot be employable for all n × n arrays. Not employable for unsymmetrical arrays.
[42], 2016	Novel-shade-dispersion (NSD)	Static, Magic-square	4 × 4	Physical relocation based on magic-square approach	Very limited analysis, compared only with TCT, Numerous compatibility issues
[24], 2018	Optimized-Sudoku (OPS)	Static, logic-Puzzle	4 × 4	Optimization of Sudoku-based scheme under mutual-shading	Limited analysis, compatibility issues, Limitations of sudoku-based techniques
[43], 2020	Diagonal-TCT (DTCT)	Static, Shift-based	4 × 4	Diagonally-dispersed- arrangement of TCT configuration	Compares only with TCT and OE, poor performance under all diagonal shadings
[44], 2020	Sudoku-puzzle (SD)	Static, logic-Puzzle	4 × 4	Two-step hybrid reconfiguration employing switching-matrix	Similar limitations of sudoku-technique, considers unrealistic shading cases,
[45], 2021	Jigsaw-puzzle (JP)	Static, Tiling-puzzle	4 × 4	Maximizes the output through physical relocation by jigsaw-puzzle pattern	Poor compatibility, malfunctions & underperforms under diagonal shading
[46], 2021	L-shaped-propagated (LSP)	Static, Analytical	4 × 4	Renumbered the PV panels in L-shaped manner	Incompatible for all arrays, ineffective under diagonal shading, low power enhancement
[47], 2016	Optimal TCT (OTCT)	Static, Zig-Zag	4 × 3	Arrangement of panels of a row into distinct parallel circuits	Poor interconnection of panels as more than half of the panels remain in same row
[47], 2016	Novel TCT (NTCT)	Static, Zig-Zag	4 × 3	Panels are reconfigured in the same column in Zig-Zag manner	Inconsistency, low power enhancement, ineffective under diagonal shading case
[48], 2022	Henon-Map (HM)	Static, Chaotic-based	9 × 9, 8 × 8, 4 × 3	Reconfigured the panels based on a generalized Henon-map matrix	Limited analysis, lack the effective shade dispersion ability for asymmetric arrays

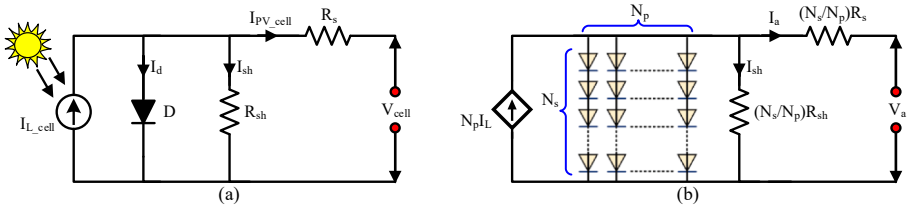

Fig. 1. (a) Equivalent circuit of a PV cell, (b) Equivalent circuit of PV array (with Ns × Np modules).

The **novelty and the major contributions of the proposed work** are presented as follows:

- For the first time, a novel reconfiguration technique employing the concept of image encryption is proposed to uniformly disperse the shade.
- The effectiveness of the proposed technique is evaluated and proved with the various encryption quality metrics.
- Unlike the existing static reconfiguration techniques that disperse the shade indiscriminately and unevenly, the proposed technique disperses intelligently by employing the encryption algorithm that reduces the correlation between the adjacent shaded panels in a row, column, and diagonal directions. Hence, the total irradiation of the rows is enhanced, and the mismatch between them is significantly reduced.
- A majority of the existing techniques (except very few) are tested only for symmetrical PV arrays. However, the proposed work considers the experimentation on both the symmetrical and unsymmetrical PV array sizes such as 9 × 9, 7 × 7, 6 × 6, 5 × 5, 4 × 4, 3 × 5, 4 × 3, 5 × 9, and 6 × 20 PV arrays.
- An inclusive comparative performance analysis of the proposed technique with the existing 41 static reconfiguration techniques is presented in detail.
- Most of the earlier research works consider only 4 to 6 shading cases and hardly 1 or 2 PV array sizes for analysis, which is quite insufficient to confirm the effectiveness of a reconfiguration technique. So, the proposed technique has been tested extensively for various array sizes under 100 shading cases which is highly adequate to confirm its efficacy.
- The experimental prototype of the proposed configuration for 4 × 4 and 3 × 5 PV arrays are developed and tested in indoor laboratory and outdoor environments under various artificially created shading conditions.
- To confirm the effectiveness and consistency of the proposed technique over the existing ones [19–48] statistically, a Non-parametric Wilcoxon signed-rank test with a significant difference of 0.05 is used for evaluation.

2. Modelling of solar PV array

A PV module constitutes the numerous cells connected in series and parallel. There exist many modeling strategies in the literature, among

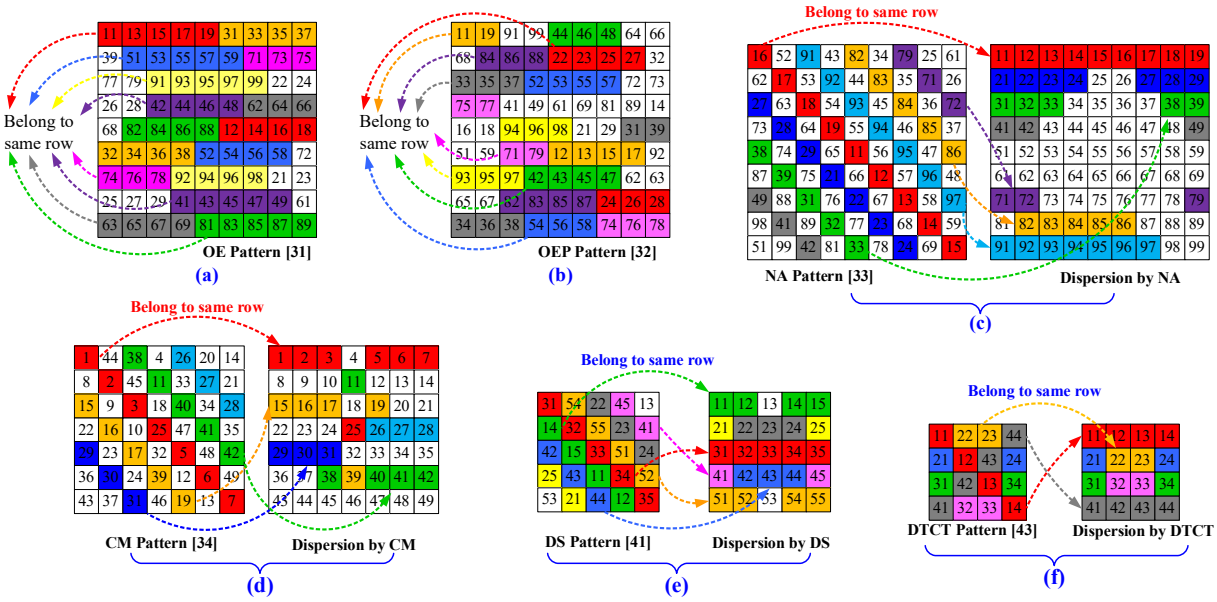

Fig. 2. Reconfigured matrix obtained by (a) OE [31], (b) OEP [32], (c) NA [33], (d) CM [34], (e) DS [41], (f) DTCT [43] and their respective shade dispersions.

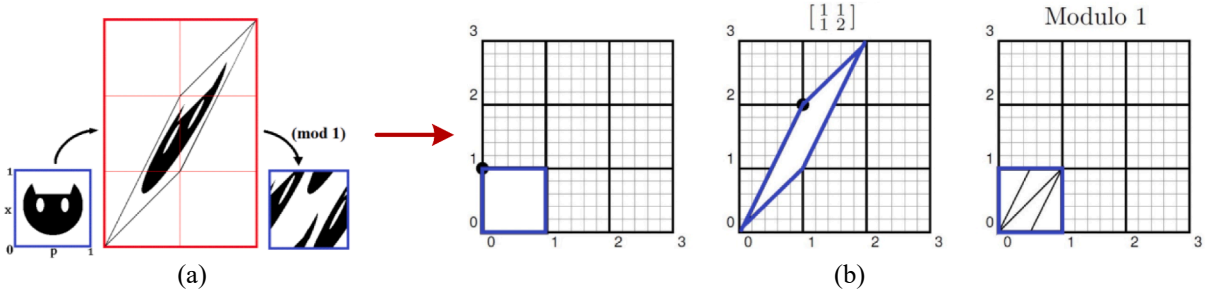

Fig. 3. (a) Description of ACM, and (b) its effect on unit square.

which the one-diode equivalent circuit model (shown in Fig. 1(a)) is widely used due to its simplicity [49]. Applying the Kirchhoff's current law, the obtained solar cell current is given as follows,

$$I_{PV\_cell} = I_{L\_cell} - I_{sh} - I_d \tag{1}$$

where I_{pv_cell} is cell current, I_{L_cell} is light- generated current of cell, I_{sh} is shunt resistance current and I_d is diode current. By substitution of I_d and I_{sh} in Eq. (1), I_{pv_cell} can be expressed [47] as.

$$I_{PV\_cell} = I_{L\_cell} - I_0\left[\exp\left(q\frac{V_{cell} + I_{PV\_cell}R_{se}}{b\sigma T_c} - 1\right)\right] - \frac{V_{cell} + I_{cell}R_{se}}{R_{sh}} \tag{2}$$

where I_o is diode saturation current, q is electron charge, V_{cell} is cell voltage, σ is ideality factor, T_c is operating temperature, b is Boltzmann's constant, R_{se} and R_{sh} are the series and shunt resistance of cell. The current of a PV module comprising 'n_s' cells in series is given as.

$$I_m = I_L - I_0\left[\exp\left(q\frac{V_m + I_mR_{SE}}{n_sb\sigma T_c} - 1\right)\right] - \frac{V_m + I_mR_{SE}}{R_{SH}} \tag{3}$$

where I_m is module current, V_m is module voltage, R_{SE} and R_{SH} are series and shunt resistance of the module, and I_L is light- generated current of module, which is expressed as given.

$$I_L = \frac{G}{G_0}[I_{L\_STC} + K_{sc}(T_c - T_0)] \tag{4}$$

where G is actual solar irradiation, G_0 is standard irradiation, I_{L_STC} is module's light-generated current under standard test condition, K_{sc} is temperature coefficient of short circuit current (I_{sc}), T_0 is standard operating temperature. The PV array consisting $N_s \times N_p$ modules is shown in Fig. 1(b). Based on the PV module output current as mentioned in Eq. (3), the array current can be expressed as shown in Eq.(5) where V_a and I_a is the output voltage and current of the array.

$$I_a = N_pI_L - N_pI_0\left[\exp\left(q\frac{V_a + \frac{N_s}{N_p}I_aR_s}{N_sn_sb\sigma T_c} - 1\right)\right] - \left[\frac{V_a + \frac{N_s}{N_p}I_aR_s}{\frac{N_s}{N_p}R_{SH}}\right] \tag{5}$$

3. Need for efficient reconfiguration approach

The major research gaps, drawbacks and the need for efficient reconfiguration approach is discussed in this section. The PV array output is enhanced significantly by reducing the impact of shading in a particular row of an array. This can be done by effective reconfiguration of the array. Indiscriminate shade dispersion through arbitrary reconfiguration doesn't result in optimal output. Further, it yields substantially lower output than conventional configurations under certain shading conditions. The best reconfiguration approach is the one that is compatible with all array sizes and exhibit uniform shade dispersal irrespective of shading pattern reducing the row current mismatch and MPPs. However, a majority of the existing approaches are not compatible with all array sizes. Specifically, the application of puzzle-based [19–26,29,36,37,40,41,44,45] and Magic square-based [30,35,42] approaches is highly limited and hence cannot be scalable to all array sizes. A Chaos Map [34] technique despite being applicable to all symmetrical

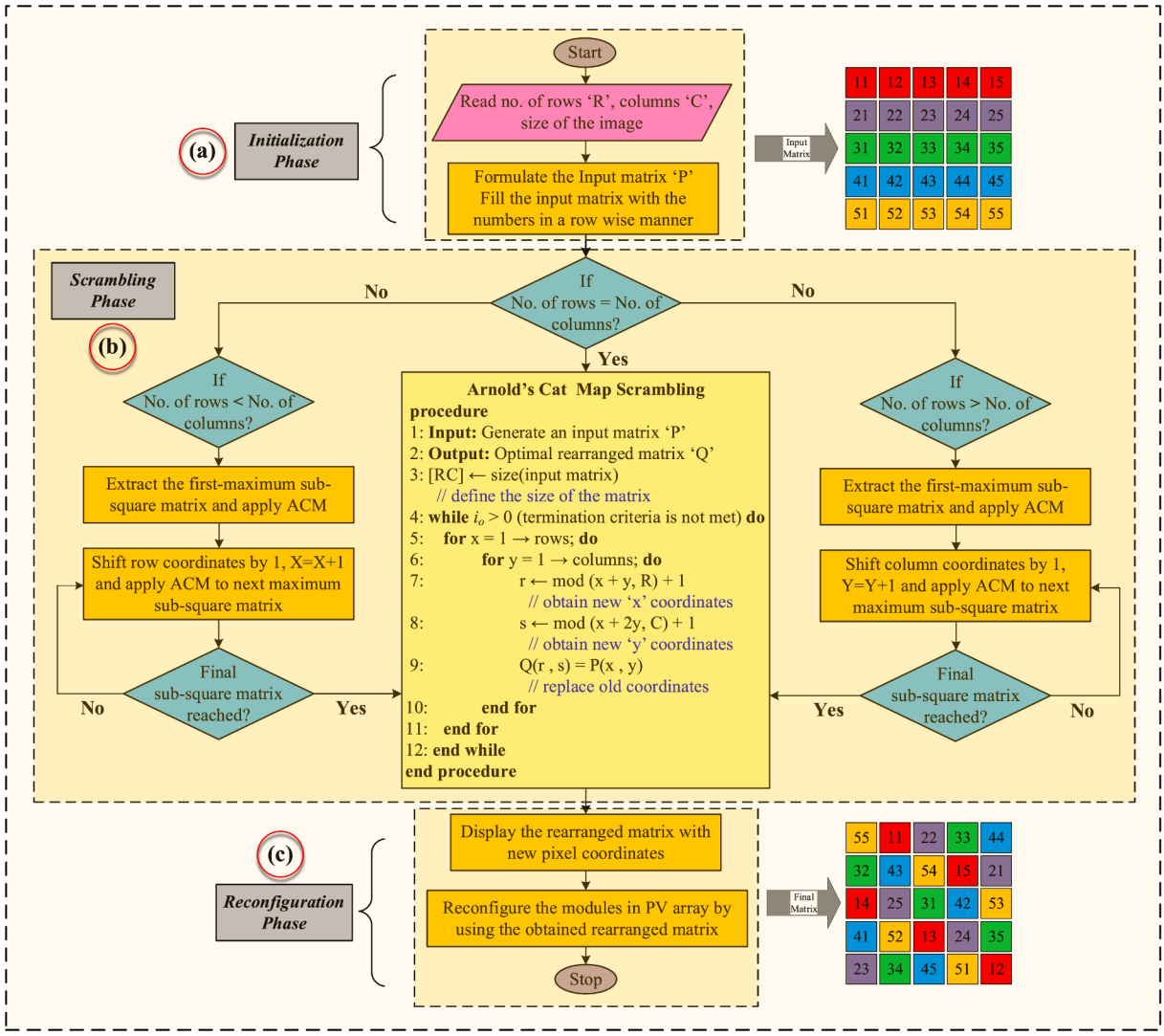

Fig. 4. Flowchart of the Generalized ACM-based reconfiguration technique.

arrays (but not for unsymmetrical arrays) has very poor shade dispersal due to high correlation between diagonal elements as shown in Fig. 2d. By reconfiguring with the CM approach, all the diagonally shaded panels will be placed in the same row as the diagonal elements of the CM pattern belong to the same row. It maximizes the mismatch between the rows significantly. Hence, it yields extremely inferior performance especially under diagonal shading and other shading conditions.

To reconfigure both symmetrical and unsymmetrical arrays, sequence-based approaches like DS [41], shift-based approaches like NA [33], and analytical-based approaches like OE [31], and OEP [32] are proposed recently. Despite their compatibility, they fail to exhibit consistent uniform shade dispersal due to their ineffective and arbitrary reconfiguration. From Fig. 2 it is evident that even after reconfiguration with DS, NA, DTCT, OE, and OEP approaches, most of the elements of a particular row or a diagonal remain in the same row resulting in poor shade dispersal under many shading cases leading to highly inferior performance. For instance, it is noted that even after reconfiguration by OE, the panel numbers 11, 13, 15, 17, 19 still belong to the same row (see Fig. 2a), and hence if the first row of the array is shaded, 56% of the row still experiences shading leading to poor performance. Similarly, even after reconfiguration by OEP, the panel numbers (22, 23, 25, 27), (52, 53, 55, 57),……etc. belong to the same row (see Fig. 2b), leading to poor shade dispersion performance. Thus, reconfiguration by OE and OEP techniques fails to yield optimal output due to their indiscriminate shade dispersal. Further, the existing NA, DS, DTCT, etc. also suffer similar limitations remarkably failing under diagonal types of shading (Fig. 2(c)-(f)). For example, a diagonal shading case where the principal diagonal panels of a 2.89 kW, 4 × 4 PV array are considered to be shaded thus receiving 400 W/m^2, and others receive 900 W/m^2. The GMP obtained under this case is 2496.1 W, whereas the GMP obtained by employing the CM, DS, and DTCT approaches are 2233.3 W, 2152.3 W, and 2152.3 W which is significantly reduced by 11.8%, 16%, 16% respectively. In order to overcome the abovementioned drawbacks, an efficient static reconfiguration approach that reduces the correlation between the adjacent shaded PV modules in a row, column, and diagonal direction is required to alleviate the shading impact in a particular row of the PV array. This significantly reduces the mismatch between the rows and enhances the array output current.

4. Proposed methodology

In recent times, there is an enormous work of employing chaotic maps in several applications of cryptography, communication, and watermarking [50]. Arnold's cat map (ACM) is the widely-used chaotic map that was introduced by Vladimir Arnold demonstrating its effects using an image of cat, performing stretching and squeezing actions in the image [51]. It is a chaotic map from the torus onto itself. Generally, a digital image is considered as a matrix of numerous pixels that have

Generalized Arnold's Cat Map Algorithm

```
// Matrix = R×C grid
// (X, Y) are the matrix coordinates
// R and C are no. of rows and columns of matrix
// K is the size of the square matrix

Procedure ACM scrambling
    1: Input: Matrix of size R, C
    2: Output: Optimal rearranged matrix
    3: totalShifts = abs(R - C) + 1;  // total number of shifts in matrix
    4: K = min(R, C);     // minimum of no. of rows and columns
    5: X = 0, Y = 0;      // initial matrix coordinates

    6: while (termination criteria is not met) do
    7: for i = 1 to totalShifts do
    8:      ACM(Matrix, X, Y, K, i)  // Apply Arnold's Cat Map algorithm
    9:      if R < C then
   10:           do X = X + 1        // shift the row coordinates by one
   11:      else
   12:           do Y = Y + 1        // shift the column coordinates by one
   13: end for

   14: ACM (Matrix, X, Y, K, shiftNumber) // takes matrix of size 'K' from (X, Y)
   14: for x = X to X + (K-1) do
   15:    for y = Y to Y + (K-1) do
   16:          r ← mod (x + y, K) + shiftNumber    // new coordinates of 'x'
   17:          s ← mod (x + 2y, K) + shiftNumber   // new coordinates of 'y'
   18:          Swap Matrix[x][y] with Matrix [r] [s]
                 //Replace old coordinates with new ones
   19:    end for
   20: end for
   21: end while
end procedure
```

Fig. 5. Pseudocode of the Generalized ACM algorithm.

integer values. When ACM is applied to encrypt an image, the pixel coordinates of a matrix are altered effectively leading to better security. Nevertheless, after sufficient iterations, the original image reappears eventually. The considered number of iterations is known as Arnold's period. The classical ACM is a two-dimensional invertible chaotic map and toral automorphism [49] defined as.$\Gamma: [0,1) \times [0,1) \to [0,1) \times [0,1)$

$$\Gamma(x, y) = (2x + y, x + y) \,(\mathrm{mod}\, 1)$$

$$\begin{pmatrix} x(n+1) \\ y(n+1) \end{pmatrix} = \begin{pmatrix} 1 & 1 \\ 1 & 2 \end{pmatrix} * \begin{pmatrix} x(n) \\ y(n) \end{pmatrix} mod\ 1 \tag{6}$$

where x(i), y(i) ∈ [0,1] and (x mod 1) indicates the fractional component of ×, and hence (x_n, y_n) is circumscribed in the unit square $[0,1)^2$. ACM is area-preserving as the cat map matrix determinant is one. Eq. (6) can be discretised as.

$$\Gamma(x, y) = (2x + y, x + y) \,(\mathrm{mod}\, N)$$

$$\begin{pmatrix} x(n+1) \\ y(n+1) \end{pmatrix} = \begin{pmatrix} 1 & 1 \\ 1 & 2 \end{pmatrix} * \begin{pmatrix} x(n) \\ y(n) \end{pmatrix} mod\ N \tag{7}$$

The generalised iterative form of ACM [49] representing a digital image I (x, y) is written as.

$$A: I(x(n), y(n)) \to I(x(n+1), y(n+1))$$

$$\text{where } \begin{pmatrix} x(n+1) \\ y(n+1) \end{pmatrix} = \begin{pmatrix} 1 & a \\ b & ab+1 \end{pmatrix} * \begin{pmatrix} x(n) \\ y(n) \end{pmatrix} mod\ N \tag{8}$$

where (x(n), y(n)) ∈ Z_N^2 denotes discrete coordinates after 'n' iteration, $A = \begin{pmatrix} 1 & a \\ b & ab+1 \end{pmatrix}$ and a ∈ Z_N and b ∈ Z_N, where a and b are control parameters. $[x(0), y(0)]^T$ are the initial pixel coordinates of an image and $[x(n), y(n)]^T$ are the pixel coordinates obtained after 'n' iterations of

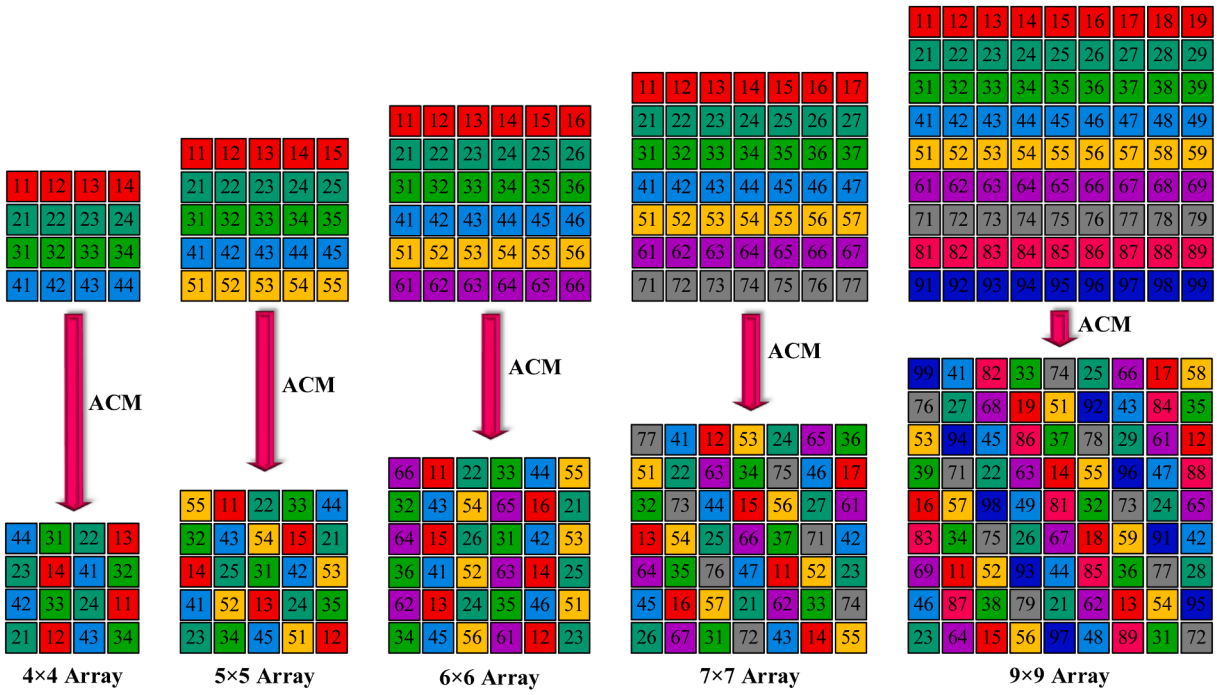

Fig. 6. Original matrices and their corresponding rearranged matrices obtained by the proposed ACM.

Table 2
Encryption quality metrics [53] of the proposed ACM for various array sizes.

Array	Correlation	MSE	PSNR	SSIM
9 × 9	−0.00004	1347.33	−31.2948	+0.00015
7 × 7	+0.0001	808.000	−29.0741	+0.00780
6 × 6	−0.0122	596.333	−27.7549	−0.02940
5 × 9	−0.0946	452.444	−26.5557	−0.07910
5 × 5	+0.0001	404.000	−26.0638	−0.04690
4 × 4	−0.0198	257.500	−24.1078	−0.01940
4 × 3	−0.0703	269.010	−24.2975	−0.04800
3 × 5	−0.1464	42.8000	−16.3144	−0.20911

ACM. The Eq. (8) of ACM reconstructs all the pixel coordinates of an image. It has two factors leading to chaotic behaviour: tension (multiply matrix to extend ×, y) and folding (applying mod to bring × & y in a unit matrix). ACM is regarded to be chaotic, with a geometrical description as shown in Fig. 3(a), from which it is noted that a unit square is stretched initially by linear transform and later folded by modulus operation.

The eigen values of Jacobian matrix 'A' of generalized ACM is $\lambda_+ = 1 + \frac{ab + \sqrt{(ab+2)^2 - 4}}{2} > 1$ and $\lambda_- = 1 + \frac{ab - \sqrt{(ab+2)^2 - 4}}{2} < 1$. The Lyapunov characteristic exponents of ACM are the eigenvalues λ_+ and λ_- of A that is given as $\lambda\pm = \frac{(3 \pm \sqrt{5})}{2}$, resulting in one of the maximum Lyapunov exponents of ACM, $\lambda_+ > 0$ and no Lyapunov exponent is equal to zero, expressing chaotic behaviour. ACM is always strongly chaotic for the values (a and b) > 0 and hence can offer superior data shuffling [52].

Besides, the shuffling effect is further enhanced by iterating Eq.(8) with the following operation.

$$\begin{pmatrix} x(n+1) \\ y(n+1) \end{pmatrix} = \begin{pmatrix} 1 & a \\ b & ab+1 \end{pmatrix}^n * \begin{pmatrix} x(n) \\ y(n) \end{pmatrix} \ mod\ N \tag{9}$$

where n ≥ 2, and Eq. (10) is the Discrete ACM (DACM) which is a generalization of ACM for discrete sets. The DACM with varying and image dependent control parameters (a,b) during the iteration [52] is obtained as.

$$\begin{pmatrix} x(k) \\ y(k) \end{pmatrix} = \begin{pmatrix} 1 & a(k-1) \\ b(k-1) & 1 + a(k-1)b(k-1) \end{pmatrix} \begin{pmatrix} x(k-1) \\ y(k-1) \end{pmatrix} \ mod\ N \tag{10}$$

where k = 1,2,3,…N_0. During permutation phase, the initial co-ordinates (x_0, y_0) and control parameters of image 'A' are fixed [52]. Then DACM is iterated to generate the orbit of (x_0, y_0):{(x_k,y_k):k = 0,1,2, …N_0} with iteration time 'N_0' long enough. Further, a(k) and b(k) are given as.

$$a(k) = A(floor(x(k) \times M) + 1, floor(y(k) \times N) + 1)$$

$$b(k) = floor(x(k) \times M) + floor(y(k) \times N) + 2)$$

Then, (x(k),y(k)) is converted into integer sequence(i(k), j(k)). And i (k) and j(k) are given as.

$$i(k) = floor(x(k) \times M) + 1,$$

$$j(k) = floor(y(k) \times N) + 1,$$

And (i(k), j(k)) must be the coordinates of a particular pixel in the matrix. If there exist reoccurred coordinates in it, only the first one is stored. Later, the pixel values of stored coordinates in 'A' are placed in a vector 'V' which is reshaped back into an M × N matrix to obtain scrambled image A_k. The flowchart of the generalized ACM-based reconfiguration technique is shown in Fig. 4. The pseudocode of the generalized ACM algorithm is shown in Fig. 5. The original and the corresponding rearranged matrices obtained by ACM are shown in Fig. 6.

Generally, the performance of any encryption technique is evaluated by various metrics [53] such as correlation, Mean Square Error (MSE), Peak signal-to-noise ratio (PSNR), and Structural Similarity Index (SSIM). The correlation coefficient value close to zero (within ±0.1 to ±0.19) indicates a very low correlation between the original and rearranged matrices. The lowest correlation coefficient represents the effectiveness of the employed encryption strategy in reducing the correlation between the adjacent pixels of an image for better security. Higher the MSE value, higher is the error. The lower the PSNR value, the higher the error between plain and encrypted matrices. Further, the lower values of SSIM indicate no structural similarity between the two

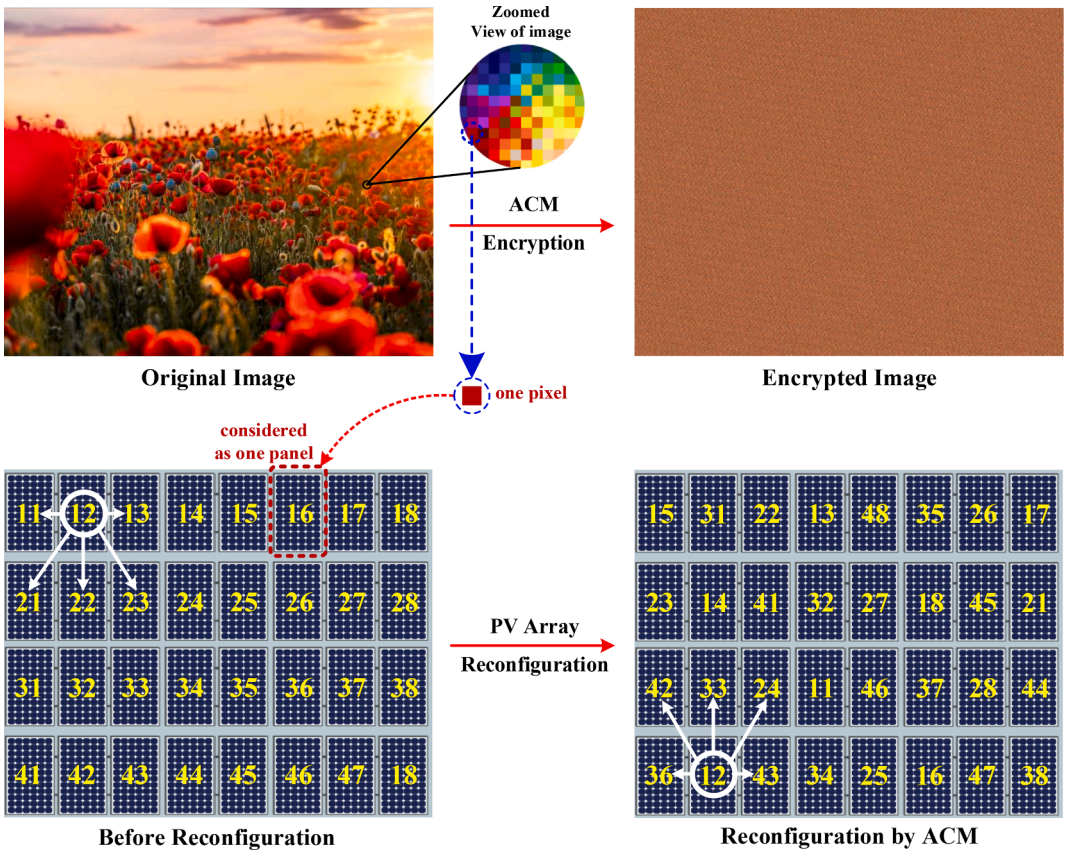

Fig. 7. Pixels of a digital image analogous to panels in PV array.

images. The best encryption strategy achieves the lowest correlation, highest MSE, lowest PSNR, and lowest SSIM. It is evident from Table 2 that the proposed ACM achieve the optimal values of these parameters.

4.1. Suitability and employment of proposed strategy in reconfiguration

As mentioned in section 3, that numerous techniques offer indiscriminate shade dispersion through arbitrary reconfiguration. Intelligent shade dispersion is the effective solution to overcome the numerous shortcomings reported by various techniques [19–48]. The concept of image encryption is employed is the best suitable solution that dispenses the shade uniformly through intelligent reconfiguration. Encryption is employed widely to ensure the security of the image by exercising various chaotic maps. When operated with a chaotic map, it intelligently repositions the original pixel locations of an image. The term 'intelligent' is used here because the algorithm makes sure that the pixels are relocated effectively reducing the correlation between adjacent pixels in a row, column and diagonal directions. The encryption concept is implemented for reconfiguration by considering an individual PV panel as a pixel of the image, and the entire PV array (of many panels) as an image consisting of pixels. By using the ACM algorithm, the PV panels are replaced intelligently according to the rearranged ACM matrix thereby reducing the correlation between the adjacent shaded panels. This mitigates the shading impacts and enhances the total row current of the array under shading.

By applying ACM, this correlation between adjacent panels in all directions is effectively reduced as illustrated in Fig. 7. Before reconfiguration, panel number 12 (PV12) is adjacent to panels PV11, PV13, PV21, PV22, and PV23 (as shown in Fig. 7). Hence, if the shade occurs in the first row of the array, due to the large mismatch between the first (shaded) row and other rows which are not shaded, the total output of the array is reduced significantly. After reconfiguration with the ACM strategy, the shading in a particular row is distributed over the entire array reducing the correlation between adjacent panels in a row of the PV array thereby mitigating the mismatch between different rows considerably. For instance, if the panel numbers PV15, PV31, PV22, PV13, PV48, PV35, PV26, PV17 of the first row of the ACM configured array is experiencing a row-type shading, then the shade is dispersed over the entire array as these panels are relocated physically in distinct rows without modifying the electric circuital interconnection of panels. Besides, the proposed reconfiguration strategy can be performed either by electrical rewiring or by physical relocation of the panels based on the obtained ACM rearranged matrix. The arrangement of panels in ACM configuration can be executed during the installation of the array itself. Moreover, it is a one-time/ fixed arrangement that doesn't necessitate further interventions, and hence it is a practical and economically feasible solution.

5. Results and discussion

The effectiveness of the proposed ACM approach has been tested and analyzed in MATLAB for various TCT configured PV array sizes such as 9×9, 7×7, 6×6, 6×20, 5×9, 5×5, 4×4, 4×3, and 3×5. The obtained results are compared with the existing and recently reported PV array configurations [19–48] under distinct shadings. A KG200GT-200 W PV panel is considered in the analysis. For simulation studies, the unshaded and shaded panels are considered to receive the irradiation of 900 W/m^2 and 400 W/m^2 respectively. The comparison of GMP for various symmetrical array sizes under distinct shading cases is given in Table 3. The comprehensive qualitative and quantitative analysis of the proposed configuration is discussed as follows:

Table 3
Comparison of GMP (in Watt) for various symmetrical array sizes under distinct shading cases.

Shading case	Array size: 9 × 9 PV array																	
	TCT [7]	SDK [19]	OS [20]	IS [21]	ADV [22]	CS [23]	MDS [23]	NOS [24]	FP [25]	OSB [26]	SMT [27]	NCI [28]	SKP [29]	LS [30]	OE [31]	OEP [32]	NA [33]	ACM
1	9068.8	11,758	12,090	11,739	11,705	11,775	11,862	11,846	11,758	11,774	11,843	11,083	11,862	11,862	10,412	11,690	11,201	**11,862**
2	10,779	11,774	12,060	11,864	11,758	11,774	11,195	11,862	12,100	12,094	11,632	11,685	11,863	11,774	10,702	10,519	11,201	**12,100**
3	10,779	11,863	11,861	12,053	11,860	11,842	11,845	11,861	11,813	11,839	11,632	11,758	11,859	11,861	11,225	10,609	11,202	**12,099**
4	10,122	9196.9	9948	10,255	10,273	9204	10,273	9841	9196.2	9603	9697.2	8868	9947.9	9960.2	7384.1	9946.5	7897.2	**10,624**
5	12,102	11,218	11,607	10,609	11,862	11,114	11,248	11,774	11,669	11,774	11,115	10,980	11,249	12,102	11,058	11,207	9641.9	**12,102**

Shading case	Array size: 7 × 7 PV array				Shading case	Array size: 6 × 6 PV array							Shading case	Array size: 5 × 5 PV array				
	SP [7]	TCT [7]	CM [34]	ACM		TCT [7]	MS [35]	KK [36]	LS [36]	AS [37]	CB [38]	ACM		TCT [7]	TT [39]	SKY [40]	DS [41]	ACM
14	6872.3	7244.1	7411.6	**7831.2**	**27**	4336.7	4644.6	4651.3	4620.6	4292.6	3895.1	**5069.6**	**40**	2748.5	2695.3	3148.9	2811.2	**3194.3**
15	6216.1	6568.5	7241.0	**7665.1**	**28**	4504.8	4504.8	4600.1	5014.4	5017.7	5014.3	**5316.8**	**41**	3195.8	3193.6	3577.8	3311.0	**3577.8**
16	7566.7	7566.7	7977.3	**8168.5**	**29**	4285.3	5316.8	5316.8	5316.8	5316.8	4913.2	**5316.8**	**42**	2666.2	2666.2	3525.9	3525.9	**3525.9**
17	4965.7	4965.7	6409.5	**6771.0**	**30**	3848.6	5051.9	5089.9	5024.6	5023.4	5017.7	**5316.8**	**43**	2674.7	2606.5	3311.0	3311.0	**3577.8**
18	6332.8	6790.5	7283.8	**7742.7**	**31**	5233.5	5643.4	5716.6	5236.8	5915.7	5716.6	**5716.6**	**44**	3362.3	3278.8	3371.2	3362.3	**3783.5**
19	7481.4	7533.7	5984.6	**7533.7**	**32**	5373.5	5120.0	5112.5	4285.3	4990.8	5111.9	**5373.5**	**45**	3579.8	3543.1	2843.2	2666.3	**3579.8**

Shading case	**Array size: 4 × 4 PV array**							
	TCT [7]	**OPS** [24]	**NSD** [42]	**DTCT** [43]	**SD** [44]	**JS** [45]	**LSH** [46]	**ACM**
53	2233.3	2496.9	2496.9	2235.7	2280.4	2496.9	2278.1	**2496.9**
54	2233.3	2496.9	2234.9	2230.2	2280.4	2496.9	2277.3	**2496.9**
55	2152.3	2280.4	2233.3	2278.1	2496.5	2496.5	2496.5	**2496.5**
56	1883.9	2197.0	2197.0	1883.9	2197.0	1885.2	1876.6	**2197.0**
57	2142.6	1867.8	1874.0	1890.0	1870.9	1871.5	1468.0	**2142.6**
58	2143.5	1871.5	1874.0	1855.5	1867.9	1865.2	2143.5	**2143.5**

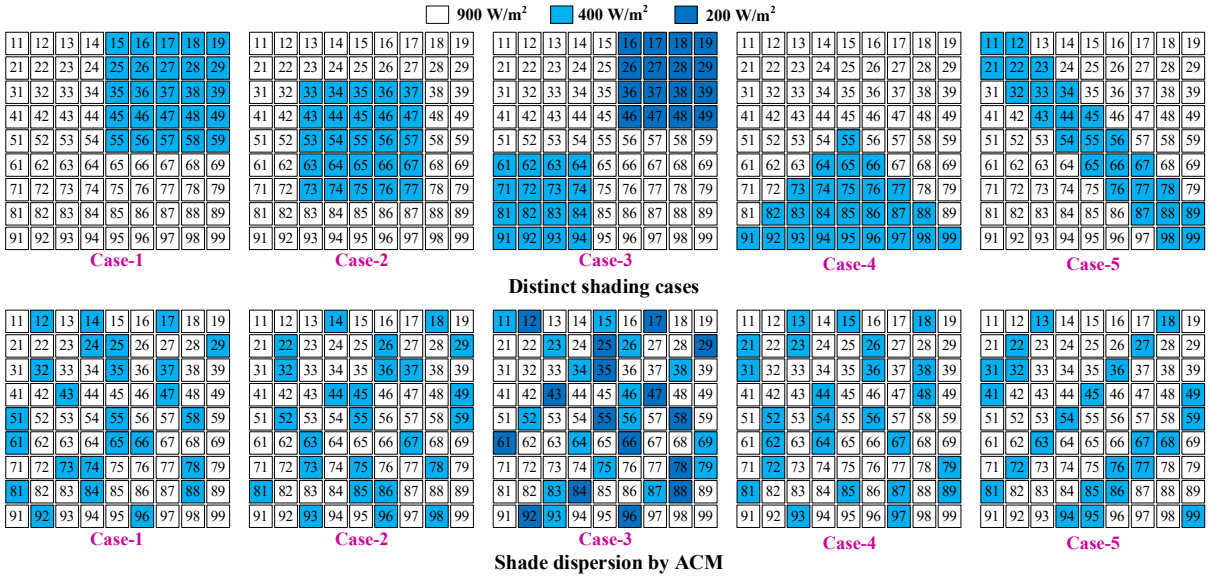

Fig. 8. Distinct shading cases and corresponding shade dispersion by ACM for a 9 × 9 array.

5.1. Analysis with 9 × 9 PV array

The proposed ACM technique uniformly distributes the shade mitigating the mismatch losses and MPPs. To verify its effectiveness, the system is tested under five distinct shading conditions as shown in Fig. 8. Further, to confirm the efficacy of ACM, its performance has been compared with the recently reported reconfiguration schemes such as SDK [19], OS [20], IS [21], ADV [22], CS [23], MDS [23], NOS [24], FP [25], OSB [26], SMT [27], NCI [28], SKP [29], LS [30], OE [31], OEP [32], NA [33] and TCT [7].

On contrary to all the existing configurations [7,19–33], ACM disperses the shade uniformly (Fig. 8) over the entire array under all the shading cases exhibiting only one or two MPPs as shown in the array PV characteristics (Fig. 9(a)-(j)). The GMP obtained by various techniques under case-1 to 5 is given in Table 4. Further, ACM enhances the output by 12.25%, 12.26%, 4.96%, and 30.81% for case-1 to case-4 respectively as shown in Fig. 10. All the existing techniques offer an inconsistent performance exhibiting enhanced output to some extent in case-1, case-2, case-4, and highly inferior performance in case-3, and case-5. During case-3 shading, the power enhancement by IS, ADV, and MDS techniques is only around 1.5%, and all the other techniques yield highly inferior output (from Fig. 10). However, ACM yields the highest output enhancing the GMP by 4.96% which is far greater than all the existing ones. During case-4, the OS technique enhances the output by 33.3% and ACM enhances by 30.81% taking second place. However, the OS technique exhibits inferior performance under case-3 and case-5, further, it is not applicable for all array sizes. Besides, under diagonal shading of case-5, all the existing techniques exhibit inferior performance even compared to conventional TCT lowering the output by a significant percentage (from Fig. 10e). Unlike existing techniques, the proposed ACM uniformly disperses the shade through effective reconfiguration exhibiting superior and consistent performance under all types of shading. The existing techniques yield reduced output and inconsistent performance due to their arbitrary reconfiguration that disperses the shade indiscriminately based on some puzzle-based or shift-based logics. To strengthen the analysis, ACM is further tested under eight more shading cases (Cases 6–13) for a 9 × 9 array and respective power enhancement is also shown in Fig. 11. ACM enhances the output by 5.97%, 0%, 18.31%, 18.63%, 18.63%, 6.31%, 0%, 15.66% under case-6 to case-13 respectively.

5.2. Analysis with 7 × 7 PV array

The proposed ACM is tested for a 7 × 7 PV array under distinct shading cases (as shown in Fig. 12) and its performance has been compared with the conventional SP [7], TCT [7] and recently reported CM [34] reconfiguration techniques. The effective shade dispersal through ACM results in delivering smooth array characteristics with only one or two power peaks as evident from Fig. 13. Besides, ACM yields the highest GMP maximizing the output by 8.11%, 16.7%, 7.96%, 36.36%, 14.03%, 0% under case-14 to case-19 respectively.

Followed by ACM, CM exhibits the respective enhancement of 2.32%, 10.24%, 5.43%, 29.00%, 7.27% under case-14 to case-18. Under case-19 (diagonal shading), the existing CM configuration delivers highly inferior performance by reducing the output by 20.57% due to its drawback of high correlation between the diagonal panels in an array. Hence, under all diagonal shading conditions, CM underperforms leading to significant mismatch and numerous MPPs thereby exhibiting inconsistent performance. The analysis is extended by considering seven more shading cases as shown in Fig. 14. ACM enhances the output by 7.96%, 0%, 27.66%, 8.24%, 14.06%, 0%, 22.04% under case-20 to case-26 respectively.

5.3. Analysis with 6 × 6 PV array

To demonstrate the effectiveness of proposed ACM for even order of symmetrical PV array sizes, a 6 × 6 PV array is considered and tested under various shading cases as shown in Fig. 15. For comparative analysis, recently reported techniques for 6 × 6 array based on MS [35], KK [36], LS [36], AS [37], CB [38] arrangements are considered.

Due to its intelligent shade dispersion over the entire array, ACM configuration exhibits uniform dispersion resulting only one power peak in four cases and two power peaks in the other two cases (from Fig. 16). It is noted from Fig. 16 that ACM shows superiorly highest performance in five out of six cases. The output obtained by ACM is considerably high compared to others under case-27, case-28, case-30, and case-32. During case-31, the AS technique yield highest output enhancing the GMP by 13.04%. Notwithstanding, AS underperforms during case-27 and case-32 resulting in lowered output by 1.02% and 7.13% respectively. Moreover, AS is not compatible with unsymmetrical PV arrays as it is based on sudoku rules which are only applicable to certain square matrices.

As in case of 9 × 9 and 7 × 7 PV arrays, the existing MS, KK, LS, AS

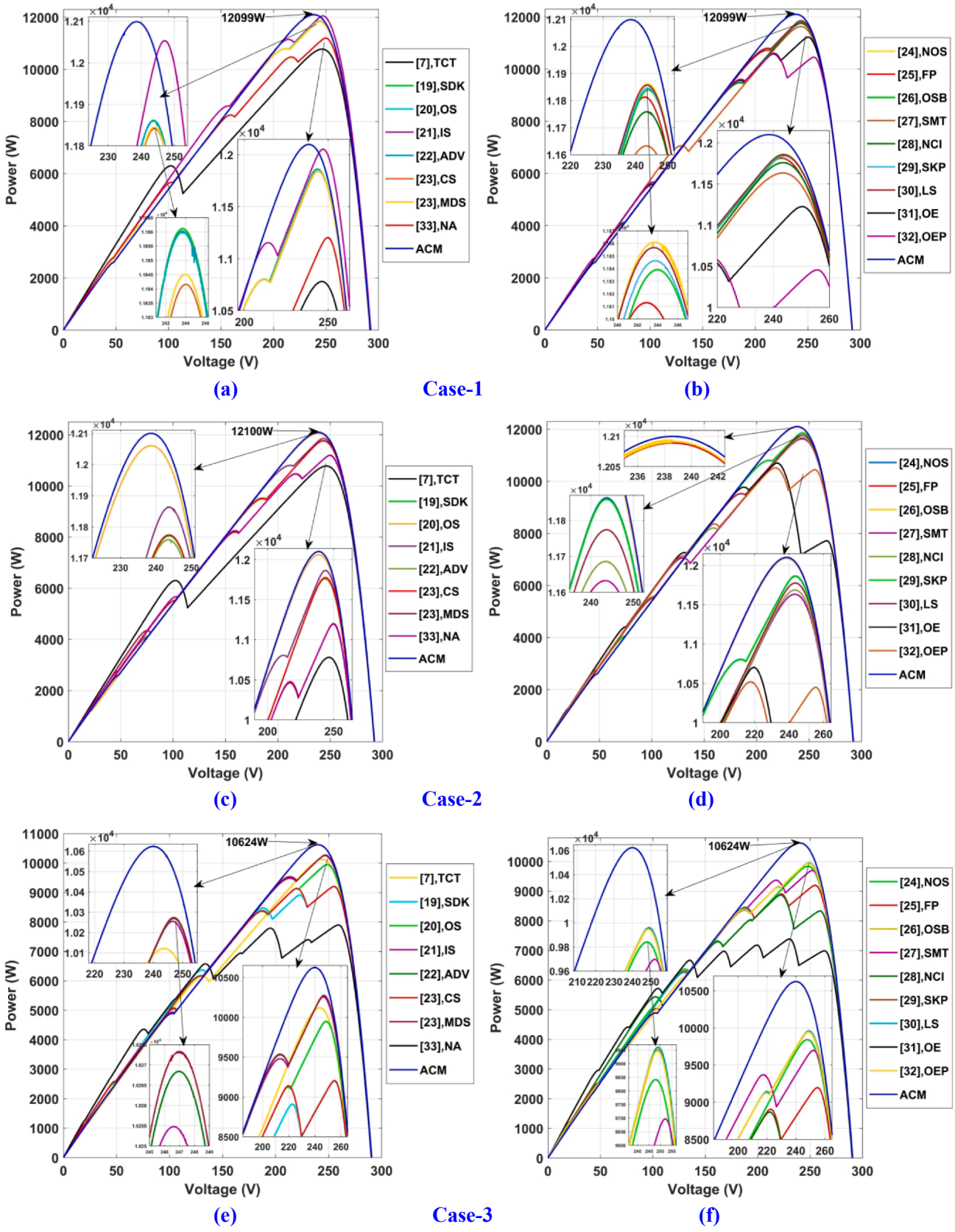

Fig. 9. PV characteristics of a 9 × 9 array under (a)-(b) Case-1, (c)-(d) Case-2, (e)-(f) Case-3, (g)-(h) Case-4, (i)-(j) Case-5.

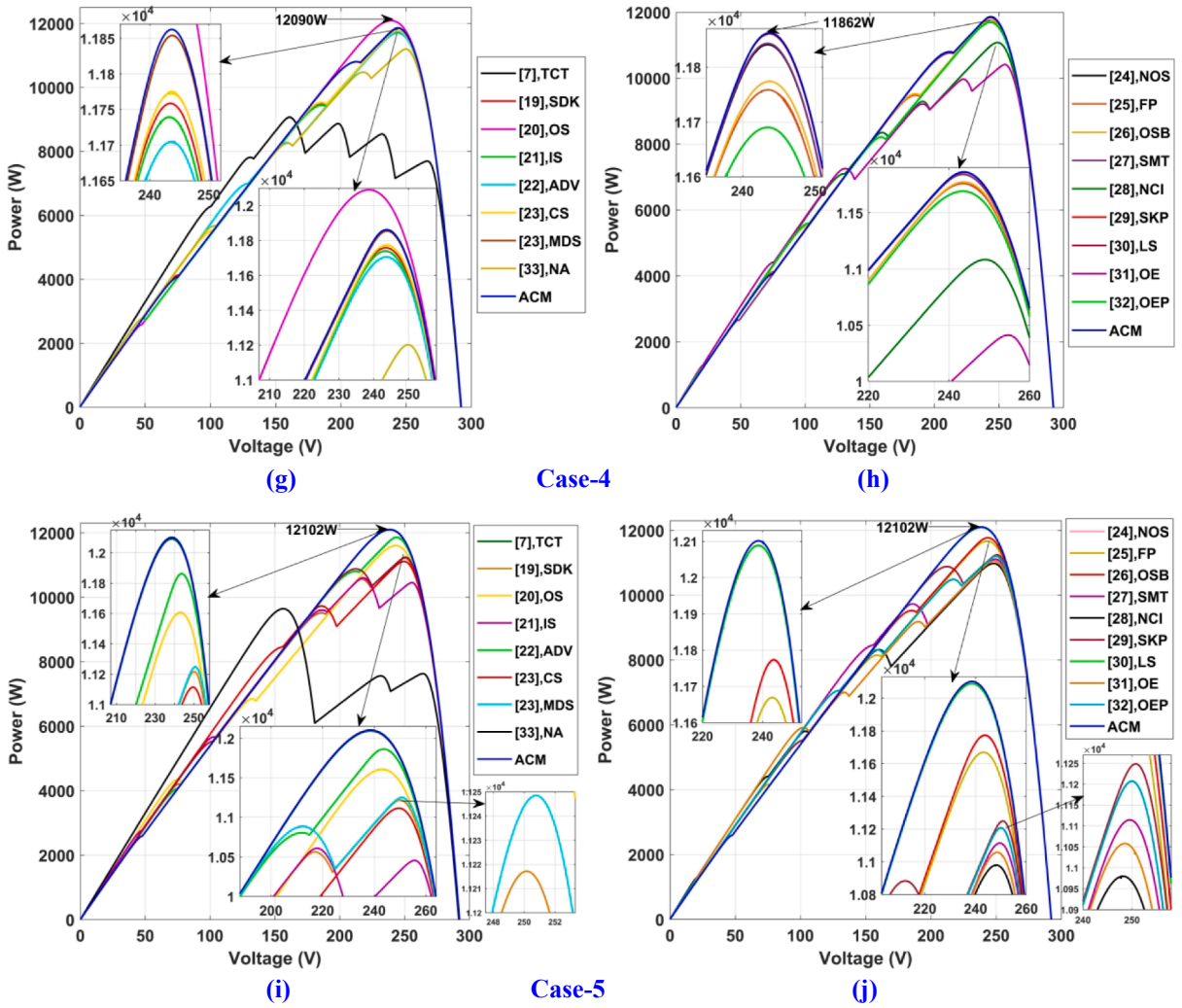

Fig. 9. (*continued*).

and CBM techniques for 6 × 6 array also significantly failed under diagonal shading (case-32) yielding −4.72%, −4.86%, −20.26%, −7.13%, −4.87% compared to benchmark TCT (from Fig. 30b). Seven more cases are considered as shown in Fig. 17 to strengthen the analysis. Once again, ACM proved its effectiveness in enhancing the GMP by 9.56%, 9.51%, 0%, 9.10%, 37.13%, 2.08%, 22.46% under case-33 to case-39.

5.4. Analysis with 5 × 5 PV array

A 5 × 5 PV array is considered to validate the effectiveness of ACM for odd order of symmetrical PV array sizes and analyzed under distinct cases as shown in Fig. 18. Recent array configurations such as TT [39], SK [40], DS [41] are considered for comparative analysis.

It is clearly evident from the PV characteristics of ACM shown in Fig. 19 that the number of MPPs are highly reduced to one or two due to its uniform shade dispersion. As shown in Fig. 24c, the ACM offers consistent performance and highest GMP enhancing the output by 16.22%, 11.96%, 32.25%, 33.77%, 12.53%, 0% under case-40 to case-45 respectively. Under diagonal shading (case-45), all the existing TT, SK, DS techniques significantly reduces the output by 1.03%, 20.6%, and 25.52% due to their ineffective reconfiguration and poor arrangement of panels. The analysis is extended by examining on seven more distinct shading cases as shown in Fig. 20. By employing ACM, the obtained GMP is enhanced by 11.96%, 11.94%, 12.53%, 56.45%, 6.35%, 1.17%, 18.90% under case-46 to case-52 respectively.

5.5. Analysis with 4 × 4 PV array

The effectiveness of ACM for small-rated PV system with 16 panels connected in a 4 × 4 PV array is investigated under various cases as shown in Fig. 21. The corresponding shade dispersion with ACM supports the smooth PV characteristics (from Fig. 22) obtained through simulation studies. To compare the supremacy of ACM, its performance has been compared with the very recently reported NSD [42], OPS [24], DTCT [43], SD [44], JS [45], LSH [46] techniques for a 4 × 4 PV array.

It is evident from Fig. 24d that ACM offers a consistently superior performance with highest GMP. Whereas, the exiting techniques [24,42–46] offer an inconsistent performance. Further, all the existing techniques underperform during left-diagonal and right-diagonal shading (case-57 and case-58) lowering the output by 13% approximately. The extended analysis for a 4 × 4 PV array is shown in Fig. 23.

5.6. Analysis with 4 × 3 PV array

For the validation of the effectiveness of the proposed technique for small-scale asymmetric arrays, a 4 × 3 PV array has been studied. The original 4 × 3 matrix pattern and the reconfigured matrix obtained by ACM is shown in Fig. 38 of Appendix. The considered array size is connected in various configurations such as TCT [7], OTCT [47], NTCT

Table 4
Comparison of GMP (in Watt) for various unsymmetrical array sizes under distinct shading cases.

Array size: 4 × 3

Shading Case	Configuration				
	TCT [7]	OTCT [47]	NTCT [47]	HM [48]	ACM
Case-66	1614.2	1529.3	1814.8	1814.8	1814.8
Case-67	1056.8	1167.4	1287.2	1287.2	1287.2
Case-68	1529.3	1529.3	1529.3	1529.3	1772.3
Case-69	1477.2	1772.3	1477.2	1515.8	1772.3
Case-70	1477.2	1515.8	1477.2	1515.8	1772.3
Case-71	1814.8	1529.3	1614.2	1529.3	1814.8
Case-72	1451.4	1116.8	1116.8	1451.4	1451.4
Case-73	1167.4	1287.2	996.97	1167.4	1287.2

Array size: 5 × 9

Shading Case	Configuration			
	TCT [7]	OE [31]	OEP [32]	ACM
Case-74	6820.2	6827.6	7501.4	7714.1
Case-75	5456.4	5504.0	5514.7	6392.4
Case-76	6471.3	6243.7	6681.5	7214.7
Case-77	4799.1	4628.1	5268.1	5683.2
Case-78	7161.1	6772.5	7178.4	7473.4
Case-79	6138.4	6046.3	5715.5	6502.8
Case-80	6269.6	6705.1	7057.2	7214.8
Case-81	7057.2	7057.2	6712.4	7214.7
Case-82	6989.1	6754.0	6846.4	7166.1
Case-83	6929.2	6783.9	6312.0	6973.5
Case-84	5929.1	6261.0	6572.9	6429.9
Case-85	5036.2	5056.0	5612.1	5803.1

Array size: 6 × 20

Shading Case	Configuration				
	TCT [7]	GA [13]	PSO [14]	HHO [16]	OE [31]
Case-86	14,100	16,333	16,530	16,443	13,526
		OEP [32]	**ACM**		
		15,150	16,467		

[47], and the very recently reported HM [48], and their performance has been compared with the proposed configuration under distinct cases (as shown in Fig. 24). The GMP obtained by these techniques under Case-66 to Case-73 are given in Table 4. It is noted from the table that two or more existing techniques yield same output under some shading cases due to similar shade dispersion resulting in the overlapping of the array characteristics as shown in Fig. 25.

The proposed technique has proved its effectiveness for symmetrical array sizes. Besides, its application and superiority over the existing techniques have also been verified for asymmetric arrays. All the existing OTCT, NTCT, and HM techniques underperformed significantly under Case-71 of diagonal shading condition resulting in a power loss of 15.73%. Further, under Case-72, both OTCT and NTCT configurations reduce the output by 23.05%. Again, during Case-73 of diagonal shading, the existing NTCT has resulted in a 14.6% power loss. The existing NTCT performed better only under Case-66 and Case-67, whereas OTCT performed better under Case-69 and Case-73. In other cases, their performance is inconsistent and not satisfactory. The recently reported HM yielded superior performance in half of the considered cases and inferior performance in other cases. Contrary to these techniques, the proposed technique manifested its superiority in yielding the highest output in all cases enhancing the GMP in the range of (10.26 to 21.8) %. Furthermore, the array characteristics obtained by the ACM configuration are significantly smoother with the least number of power peaks compared to the existing ones. This makes the tracking easy and simple for the MPPT trackers while discriminating between the local and global maximum power peaks.

5.7. Analysis with 5 × 9 PV array

A considerably large-scale asymmetric PV array with 45 panels connected in a 5 × 9 array is considered for analysis. The rearranged 5 × 9 matrix pattern obtained by ACM is shown in Fig. 38 of Appendix. The array is configured in ACM arrangement to effectively disperse the shade for mitigating the mismatch between the row currents of array. To confirm the efficacy, its performance has been compared with the recently reported OE [31] and OEP [32] techniques under 12 distinct shading cases as shown in Fig. 26.

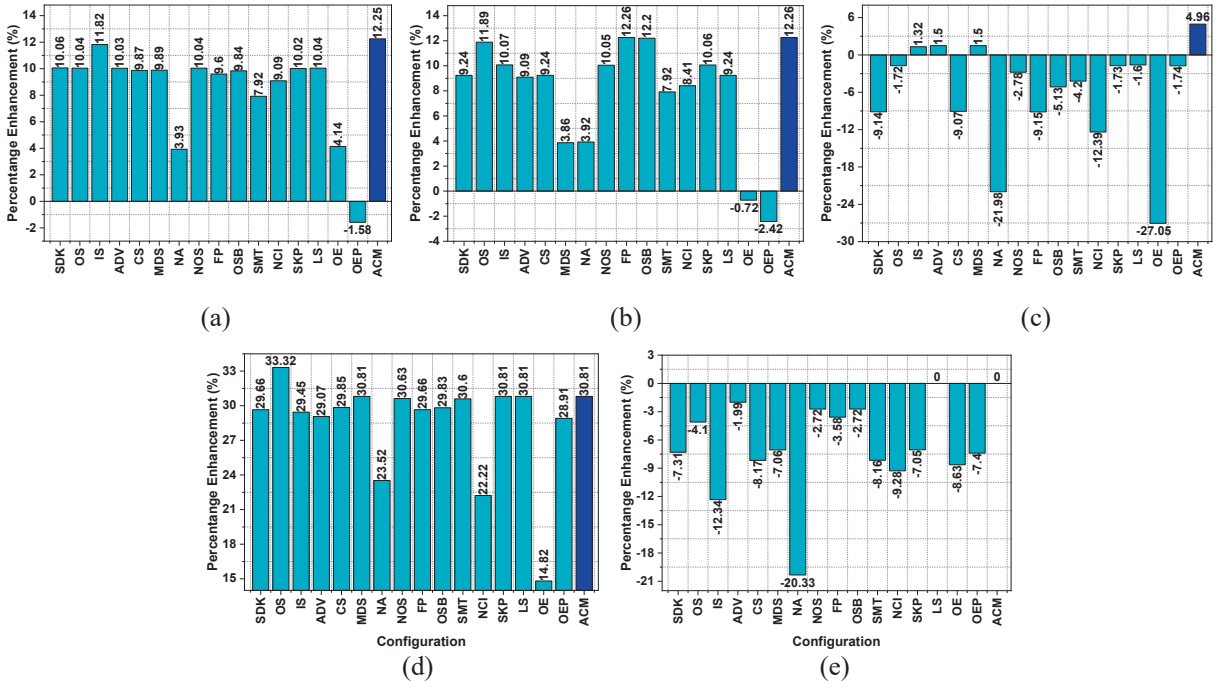

Fig. 10. Percentage enhancement in GMP under (a) case-1 to (e) case-5 respectively.

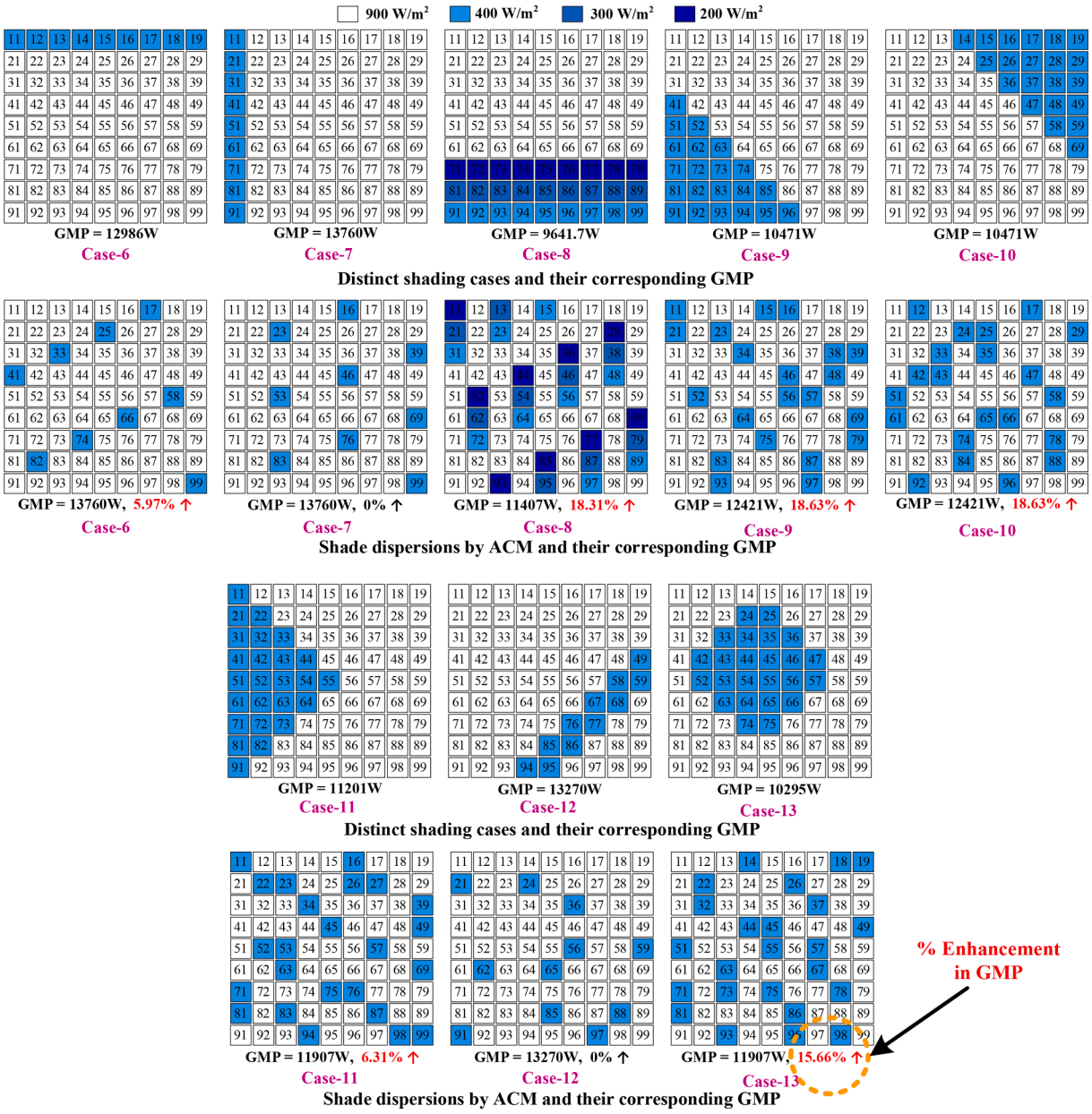

Fig. 11. Additional shading cases considered for a 9 × 9 array.

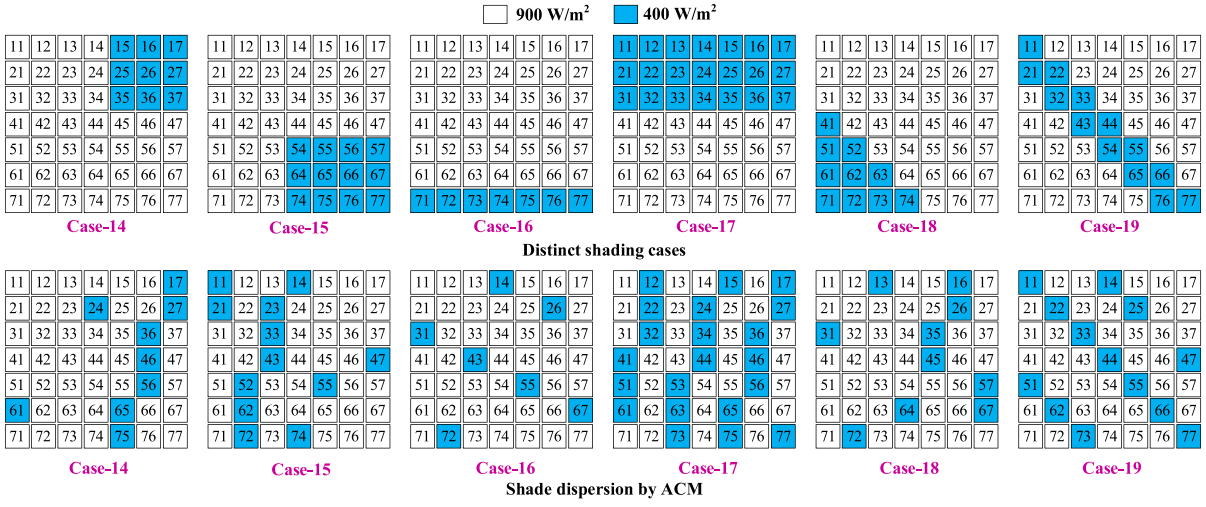

Fig. 12. Distinct shading cases and corresponding shade dispersion by ACM for a 7 × 7 array.

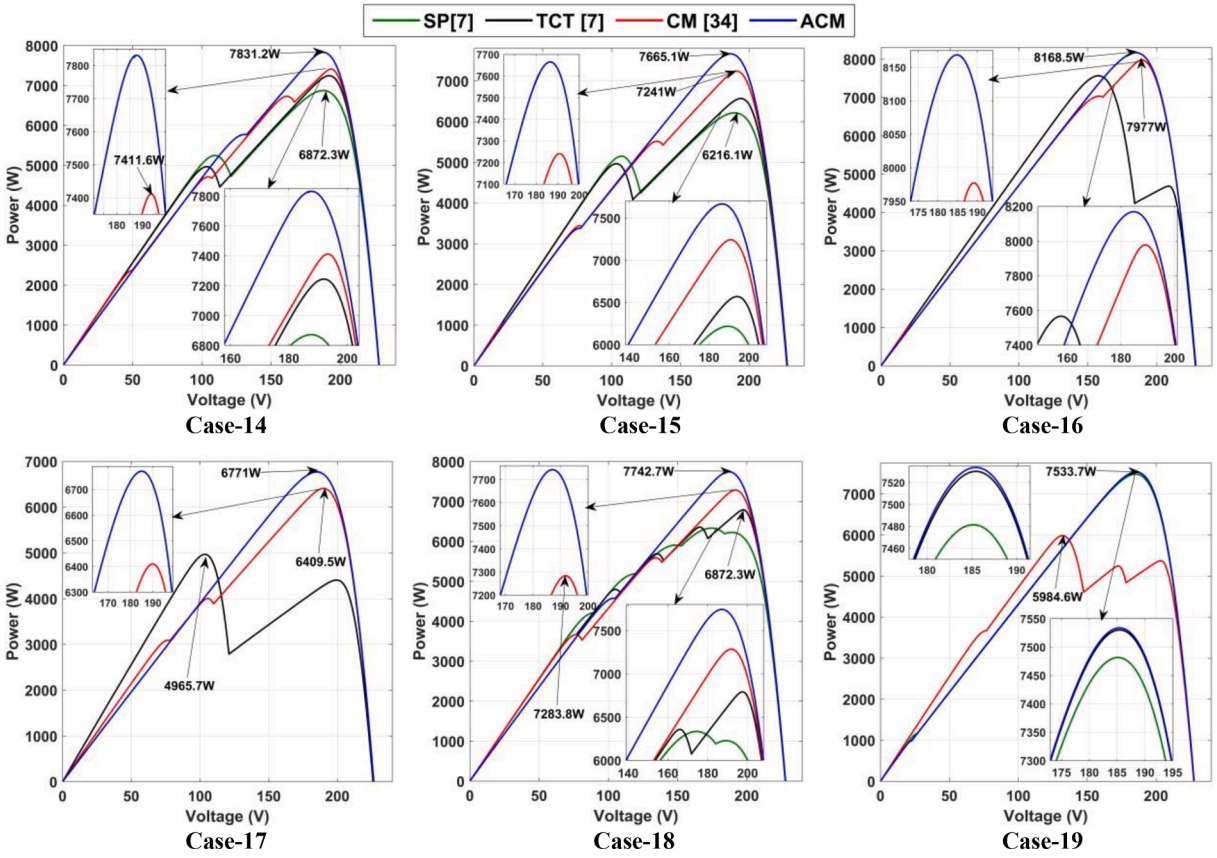

Fig. 13. PV characteristics of a 7 × 7 array under Case-14 to Case-19.

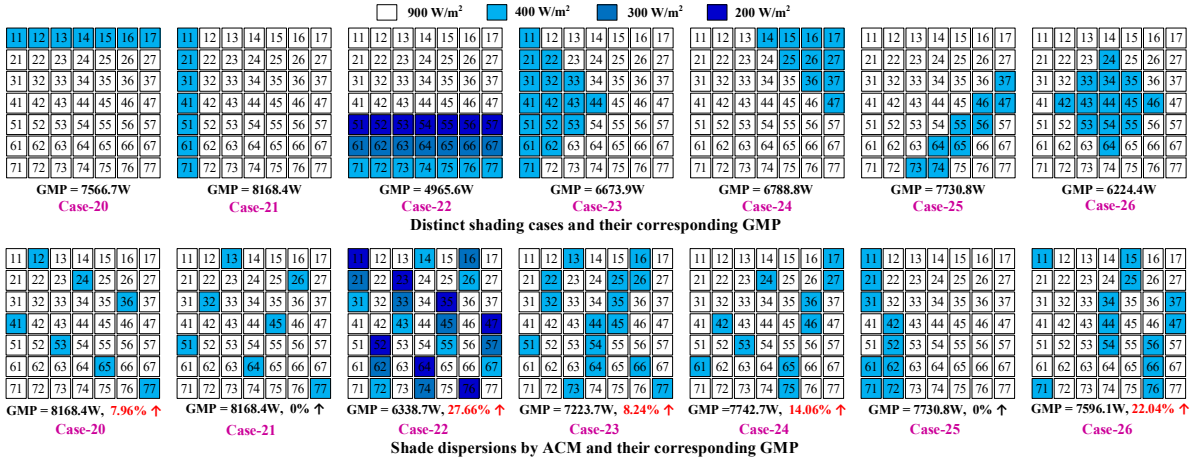

Fig. 14. Additional shading cases considered for a 7 × 7 array.

The GMP obtained by these techniques under Case-74 to Case-85 are given in Table 4. It is noted from Fig. 26 that the proposed technique disperses the shade evenly under all shading cases. The generalizability and the efficacy of ACM are once again confirmed through this analysis. Due to even shade dispersion by ACM, there exist only one or two power peaks (from Fig. 27) during almost all shading cases and the output is also significantly enhanced. The average percentage enhancement obtained by the proposed configuration is 9.56%.

In contrast, the existing OE exhibited superior performance under only two shading cases (Case-80 and 84) resulting in highly inferior performance. Besides, the OEP also exhibited better performance under only five shading cases (Cases-74, 77 80, 84, 85) yielding highly inconsistent performance. It is evident from the PV characteristics shown in Fig. 27 that the OE and OEP techniques exhibit numerous MPPs due to their indiscriminate dispersal of shade. This imposes a tremendous burden on the MPPT system in tracking the GMP. Hence, the

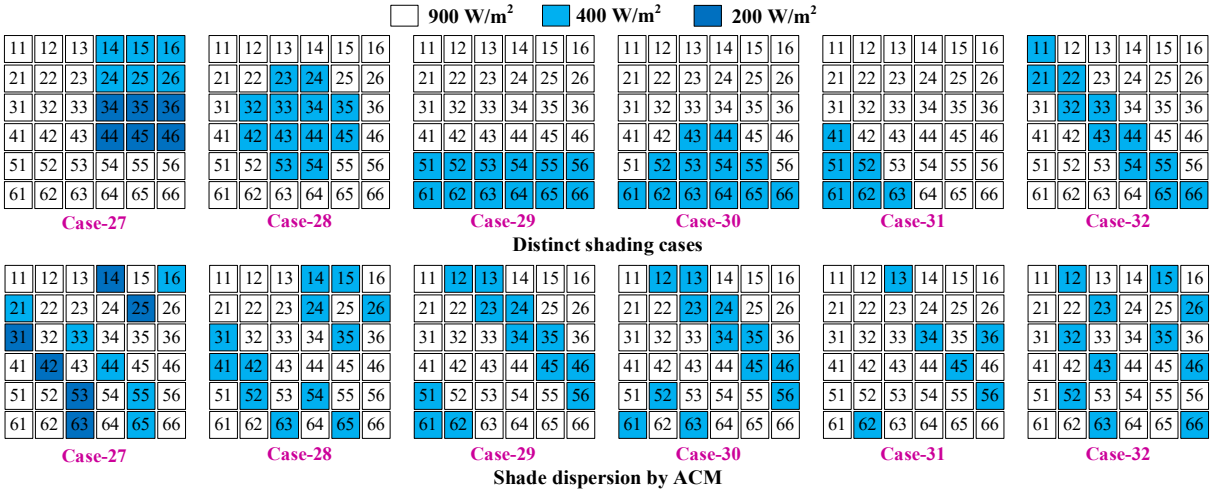

Fig. 15. Distinct shading cases and corresponding shade dispersion by ACM for a 6 × 6 array.

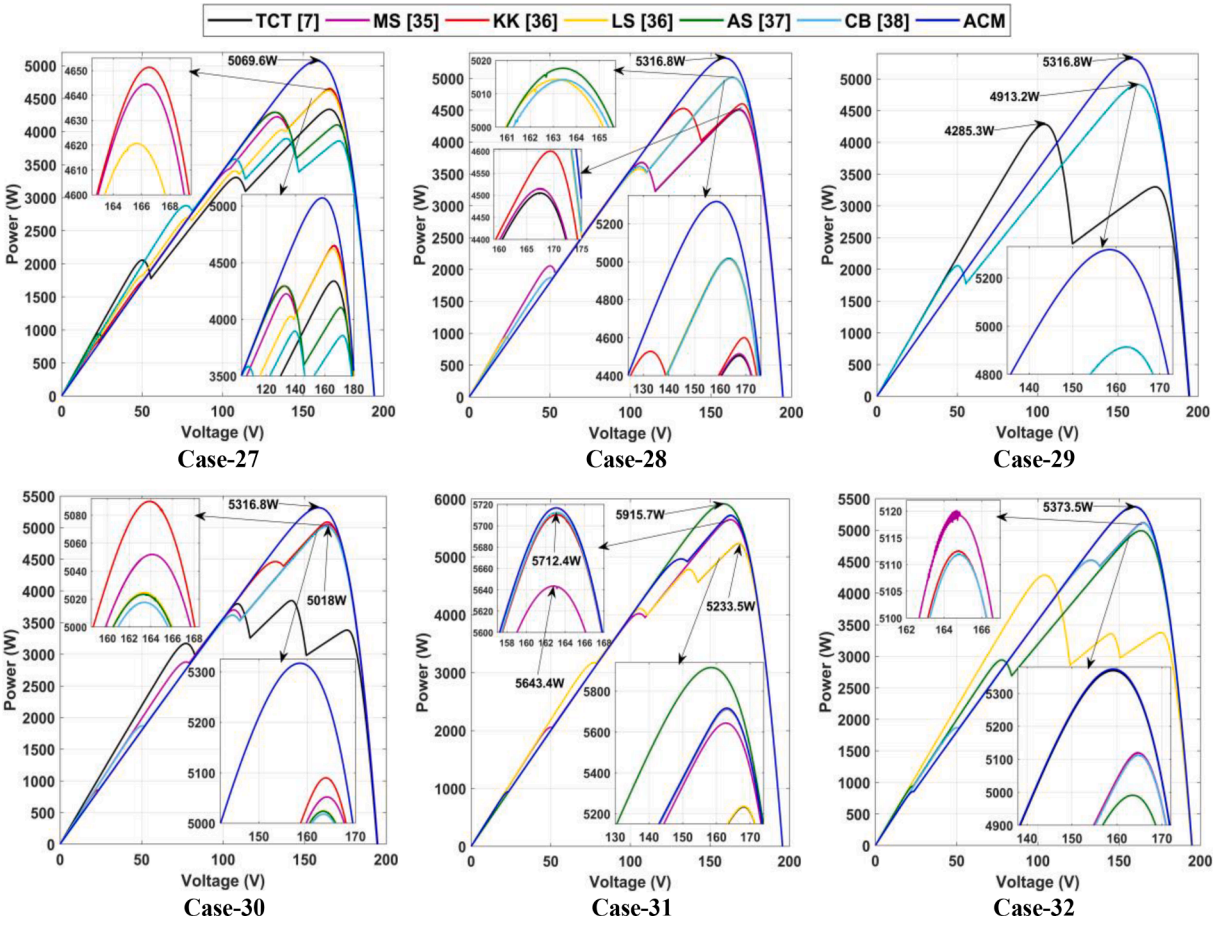

Fig. 16. PV characteristics of a 6 × 6 array under Case-27 to Case-32.

proposed strategy is considered to be effective for reconfiguring the array of any sizing.

5.8. Analysis with 6 × 20 PV array

Very recently, various metaheuristic algorithms have been reported for determining the optimal switching matrix pattern arrangement of panels for dynamically reconfiguring the PV array. A majority of these algorithms are tested only for a symmetrical 9 × 9 array and very few research papers have demonstrated the effectiveness of the algorithm for an asymmetric array. In [16], the effectiveness of the methodology is tested for an asymmetric 6 × 20 array size under a particular shading

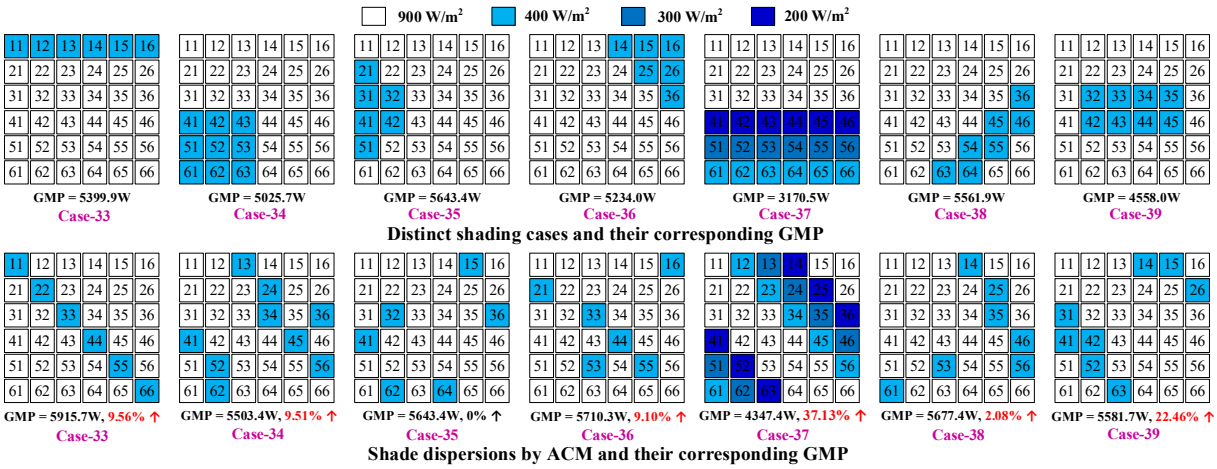

Fig. 17. Additional shading cases considered for a 6 × 6 array.

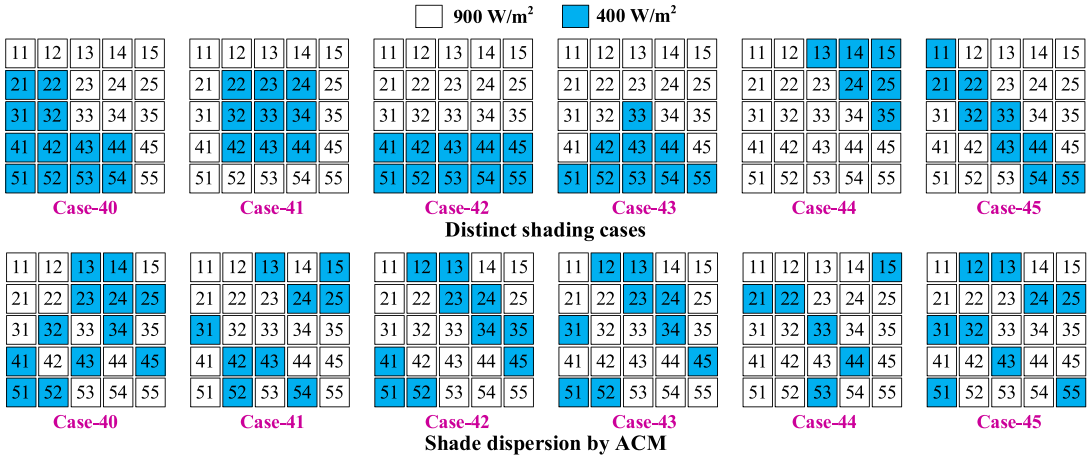

Fig. 18. Distinct shading cases and corresponding shade dispersion by ACM for a 5 × 5 array.

case. So, in order to validate the effectiveness of ACM for significantly large-scale PV arrays, we have also considered the 6 × 20 array and verified it under the same shading condition as shown in Fig. 28. The obtained results of proposed ACM are compared with GA [13], PSO [14], HHO [16], OE [31], and OEP [32] techniques.

The GMP obtained by TCT, GA, PSO, HHO, OE, OEP, and ACM techniques is 14100 W, 16333 W, 16530 W, 16443 W, 13526 W, 15150 W, 16467 W respectively. It is noted from Fig. 29 that the highest GMP is obtained by PSO, followed by ACM, HHO, GA, OEP, and OE techniques. The performance of the proposed configuration is almost on par with PSO, HHO, and GA and it is noteworthy to state that the proposed technique is also able to compete with the existing metaheuristic algorithms. Nevertheless, as mentioned in Section.1 of the introduction, the metaheuristic algorithms despite being efficient suffer numerous limitations. It is also noted in Fig. 29 that the array characteristics are significantly improved with the ACM strategy exhibiting the least number of MPPs.

The power enhancement of all the considered symmetrical and unsymmetrical PV arrays under various shading cases is shown in Fig. 30.

5.9. Experimental validation of proposed method

The developed experimental setup of the laboratory prototype model of a 4 × 4 PV array reconfiguration system to justify the simulation results is shown in Fig. 31(a). A sixteen number of 3-Watt panels are connected to form a 4 × 4 array in various configurations using banana plug connectors and interconnection wires. The artificial lighting sources (S1 to S4) that constitute multiple halogen bulbs emulating the sunlight are used to energize the panels. A 300 Ω, 1.5 Ampere variable sliding rheostat connected at the array terminals is adjusted to extract maximum output from the array. Two SM7023A digital multimeters are used to measure the array current flowing through the rheostat and the array voltage. The irradiation obtained from the artificial light source is measured by using a portable TM-206 Solar Power Meter. Further, the operating temperature of the panels is measured by an HTD8813C digital infrared thermometer gun. The irradiation obtained by each lighting source is 300 W/m^2 approximately during normal conditions.

The artificial shading of the panels is created by using various thin transparent sheets to limit the irradiation reaching the panels. The measured irradiation and temperature of the shaded panels are found to be around 160 W/m^2 and 33 °C respectively. The PV array is connected

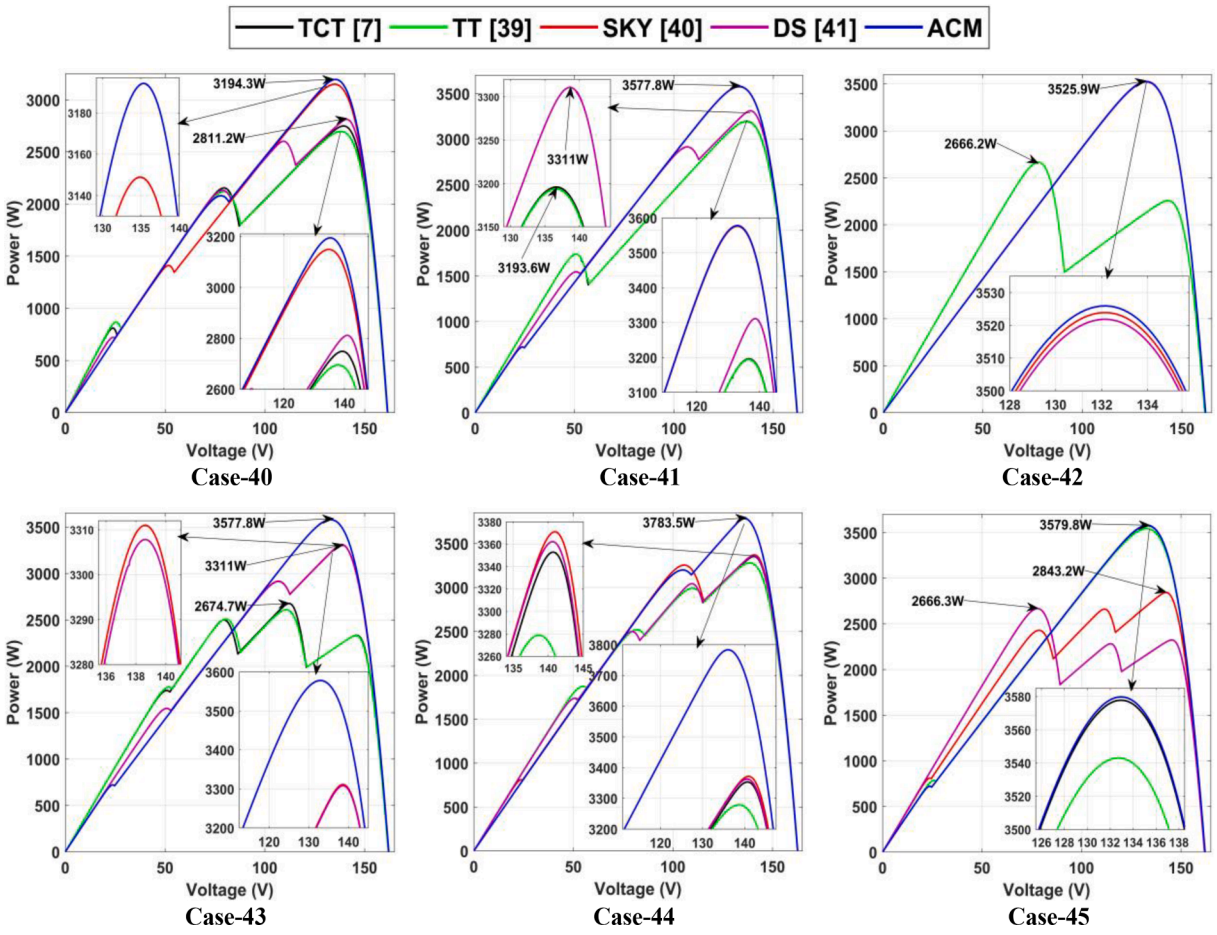

Fig. 19. PV characteristics of a 5 × 5 array under Case-40 to Case-45.

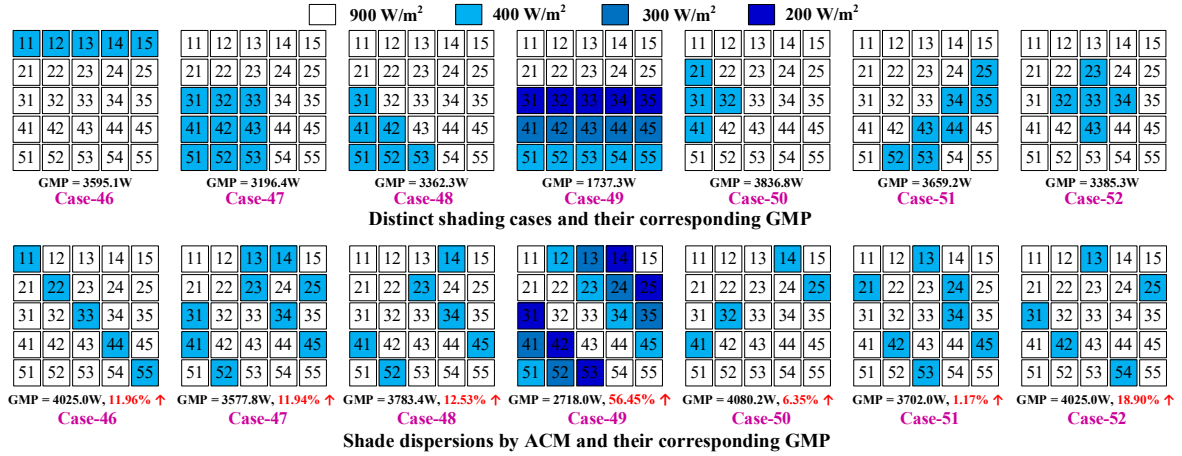

Fig. 20. Additional shading cases considered for a 5 × 5 array.

in conventional TCT and proposed ACM configurations and experimented under various shading cases as shown in Fig. 33(a). For practical realization, the ACM is also verified in the outdoor environment (see Fig. 31(b)) for an unsymmetrical 3 × 5 array under various shading conditions as shown in Fig. 33(b). The effectiveness of the ACM is compared with the recently reported OE [31] and OEP [32] techniques. In the outdoor experimental setup, the measured respective irradiation of the unshaded and shaded panels is found to be 700 W/m^2 and 250 W/m^2.

The original 3 × 5 matrix and the corresponding rearranged matrices

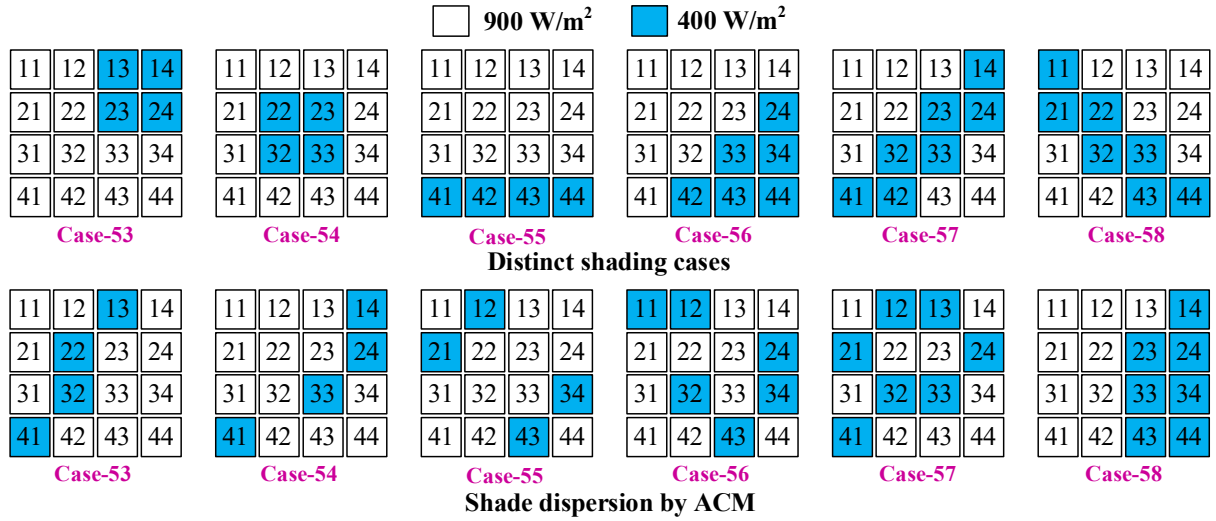

Fig. 21. Distinct shading cases and corresponding shade dispersion by ACM for a 4 × 4 array.

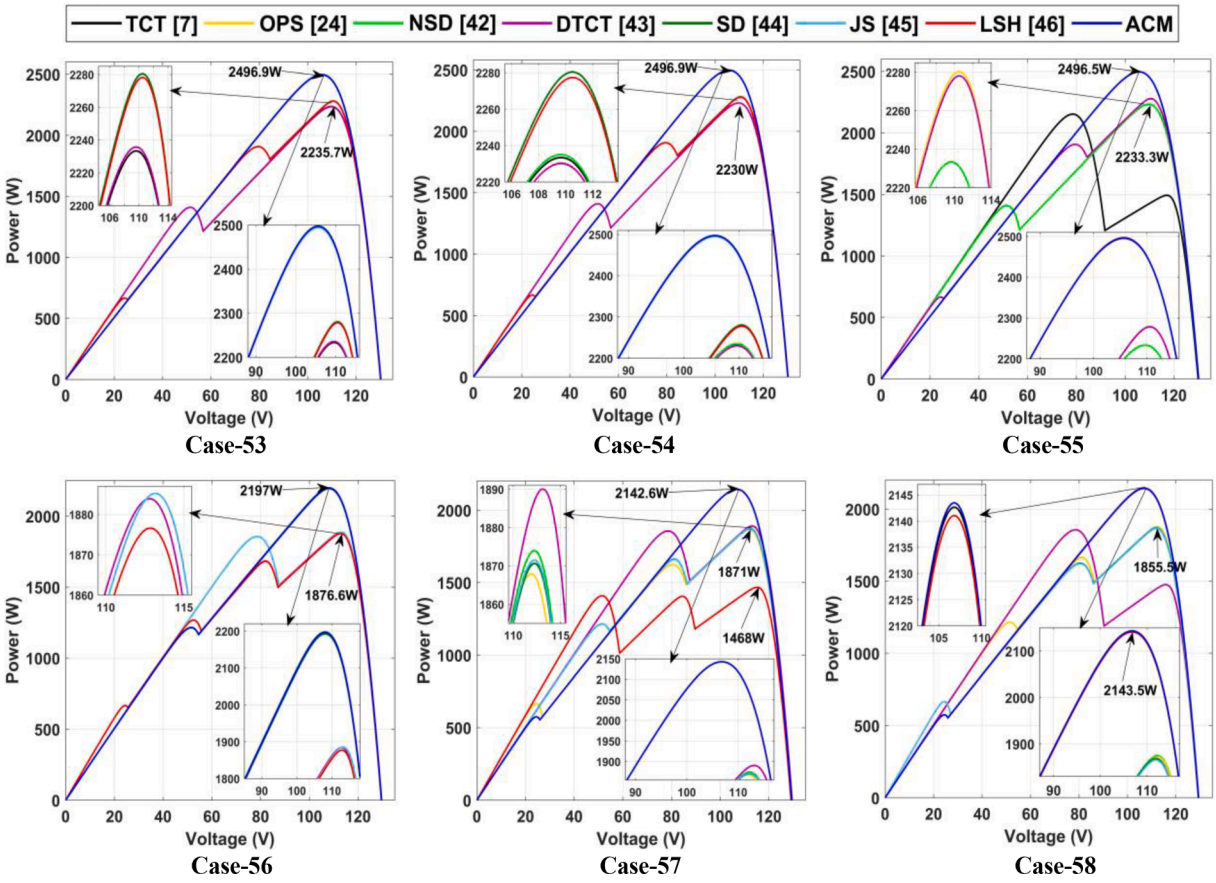

Fig. 22. PV characteristics of a 4 × 4 array under Case-53 to Case-58.

obtained by OE, OEP and ACM is shown in Fig. 32. The comparative experimental results of output power of 4 × 4 and 3 × 5 arrays under various cases are shown in Fig. 34. Besides, the PV characteristics of 4 × 4 and 3 × 5 arrays under Case-87 to Case-100 are shown in Figs. 35 and 36. During all the experimented cases, the highest GMP is obtained by ACM due to its uniform shade dispersion. On the contrary, the existing OE and OEP, despite being applicable to unsymmetrical arrays exhibit highly inferior performance due to their arbitrary reconfiguration

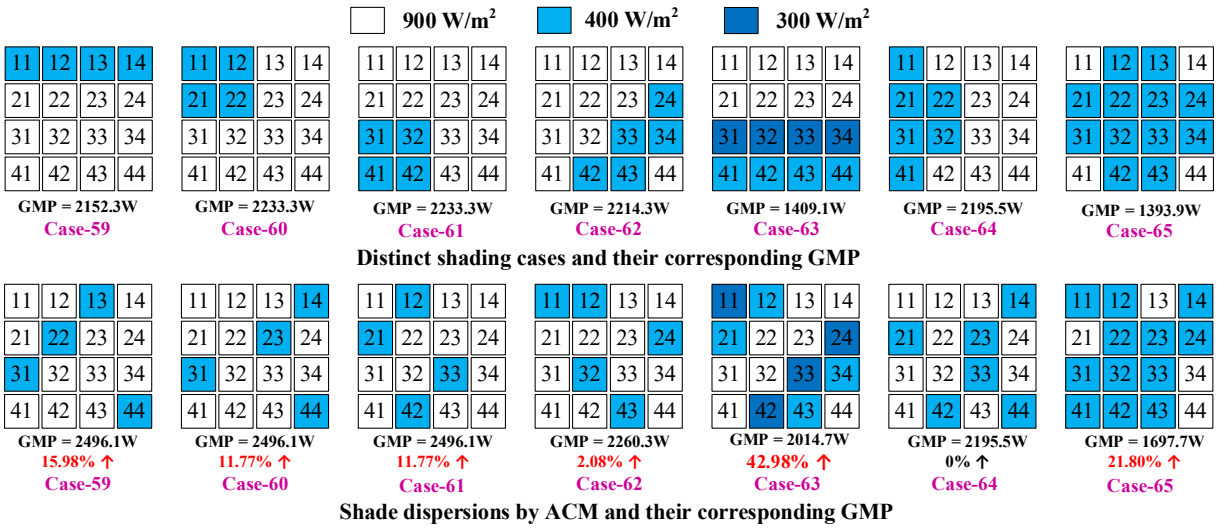

Fig. 23. Additional shading cases considered for a 4 × 4 array.

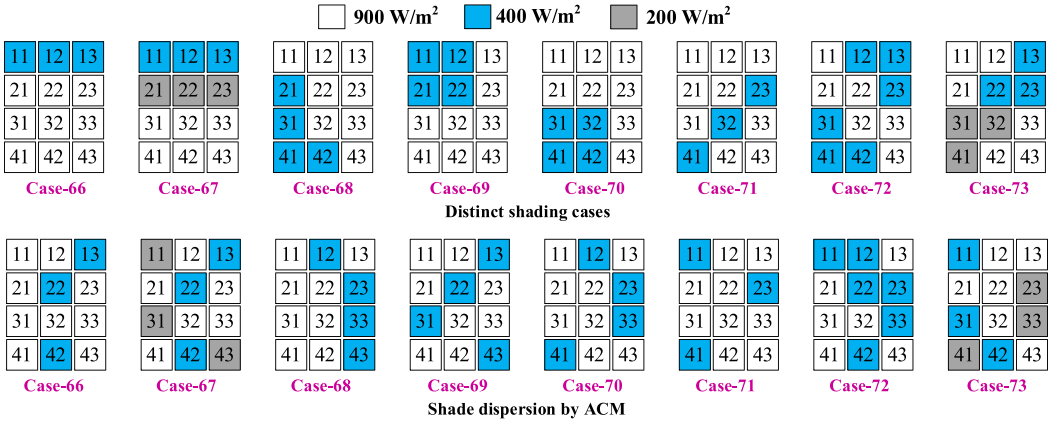

Fig. 24. Distinct shading cases and corresponding shade dispersion by ACM for a 4 × 3 array.

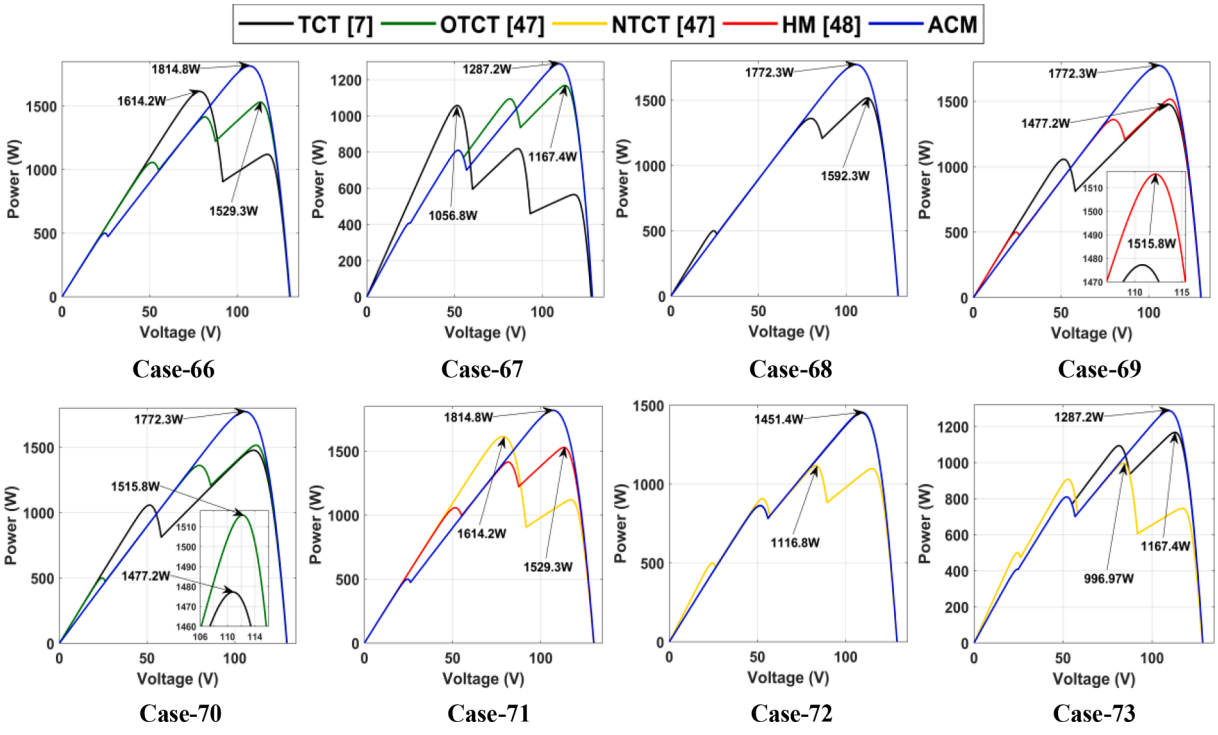

Fig. 25. PV characteristics of a 4 × 3 array under Case-66 to Case-73.

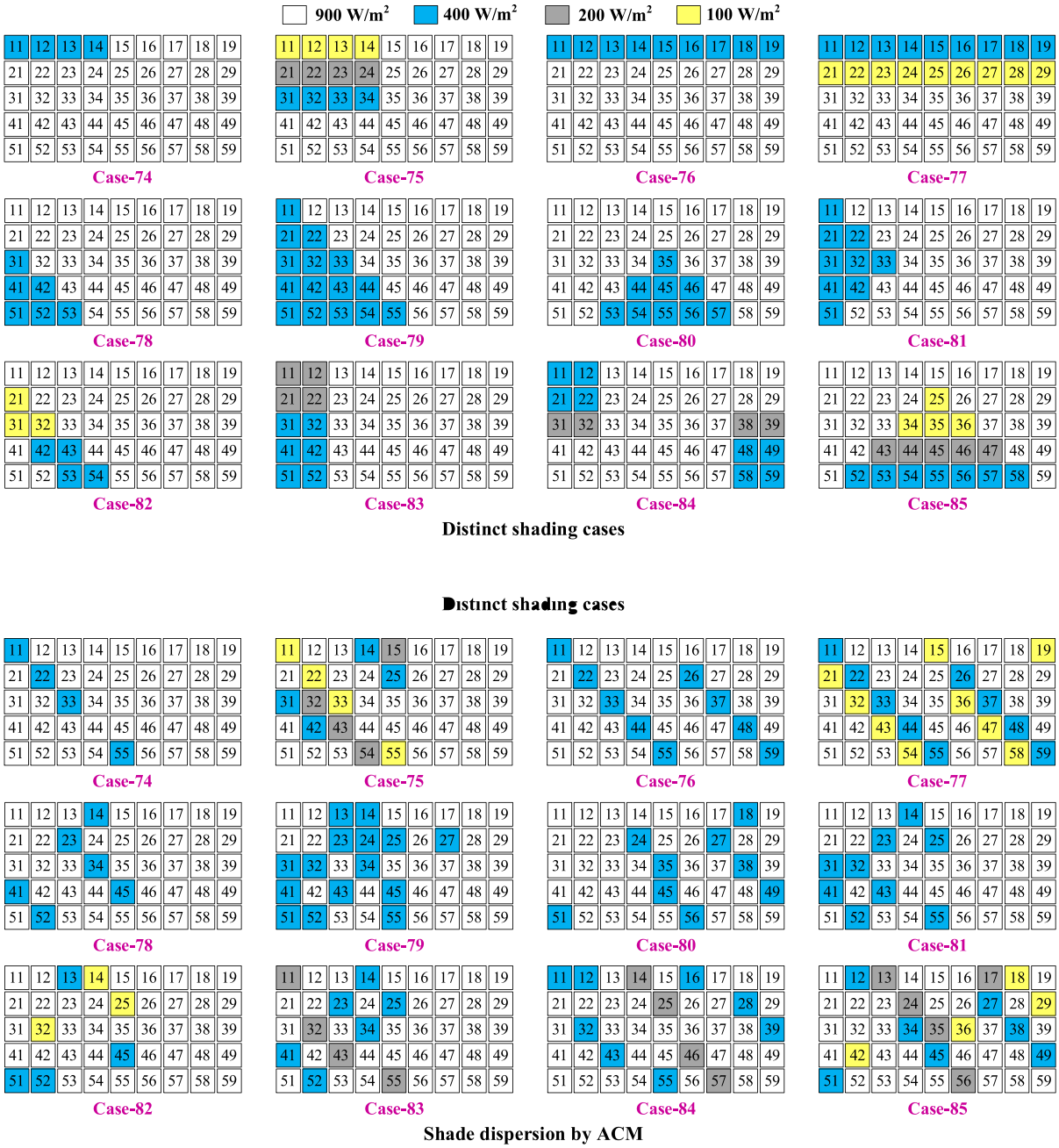

Fig. 26. Distinct shading cases and corresponding shade dispersion by ACM for a 5 × 9 array.

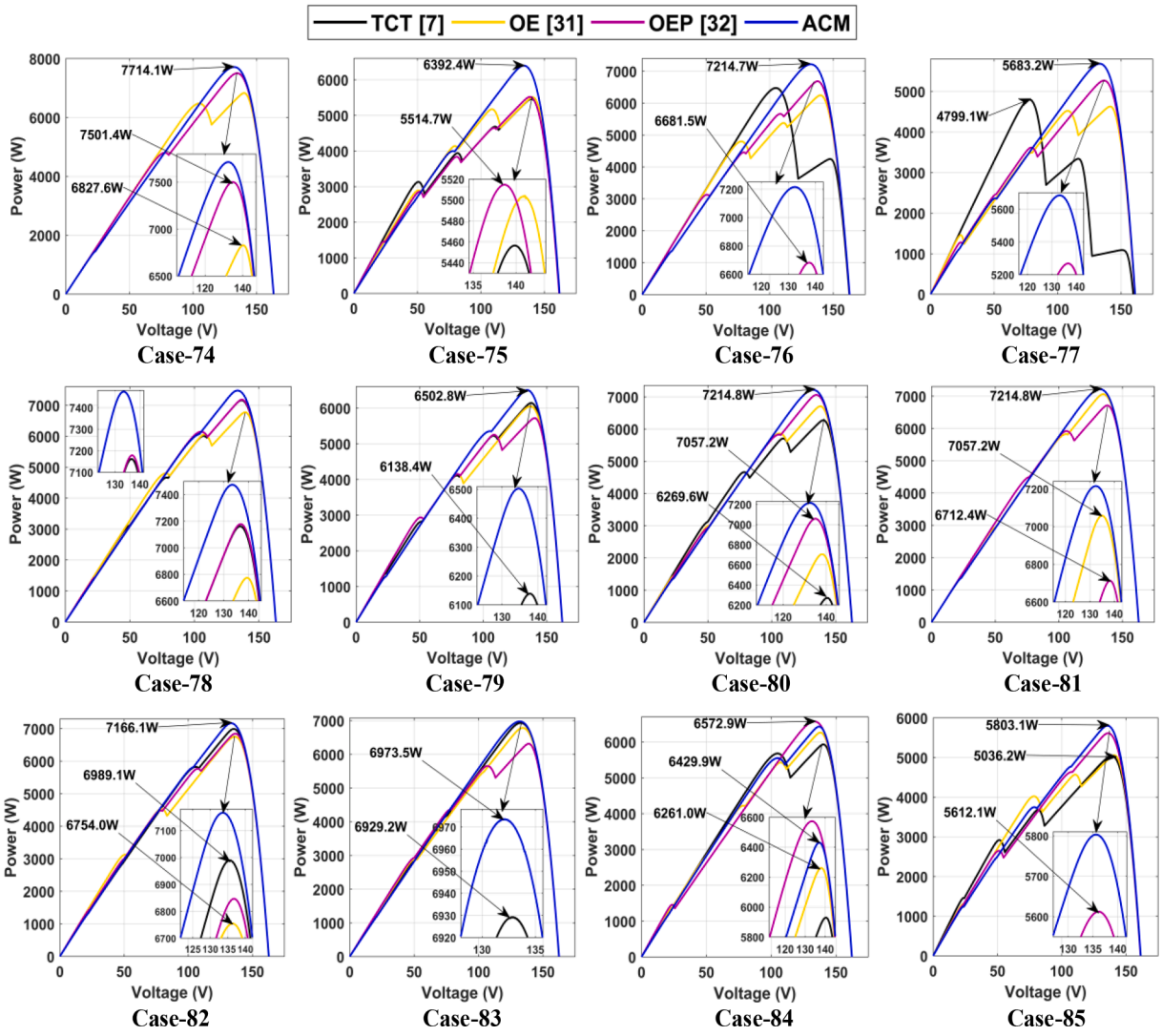

Fig. 27. PV characteristics of a 5 × 9 array under Case-74 to Case-85.

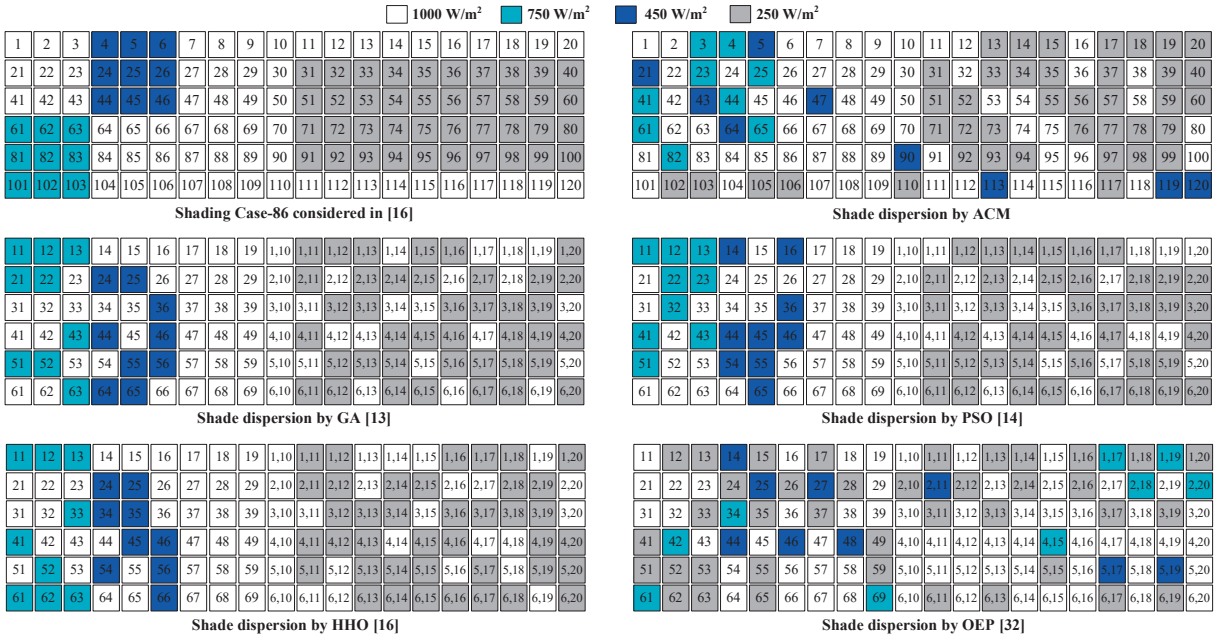

Fig. 28. Shading case-86 [16] and corresponding shade dispersion by ACM, GA, PSO, HHO, OEP.

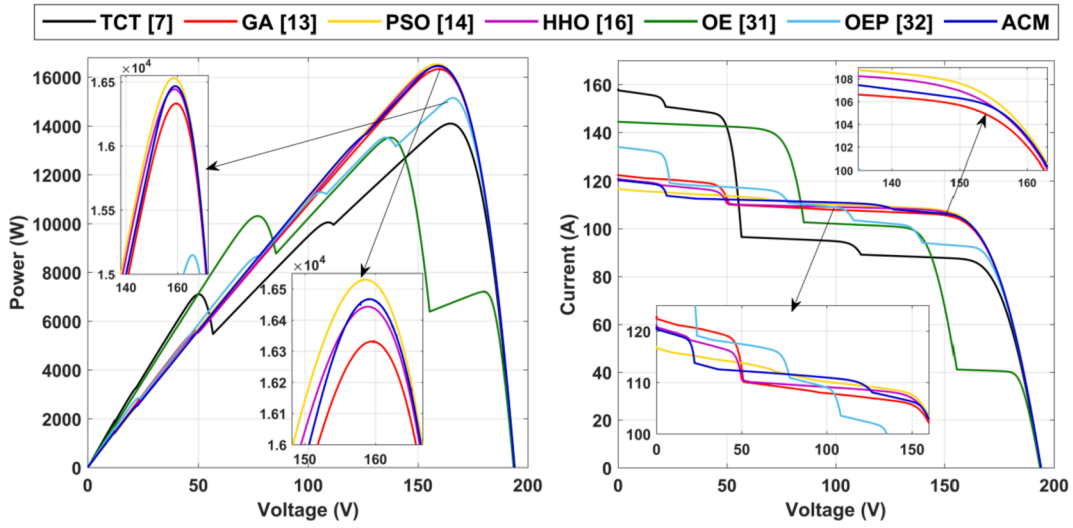

Fig. 29. PV and IV characteristics of a 6 × 20 array under Case-86.

approach. It is noted from Fig. 34(b) that both OE and OEP techniques enhances the output only in one case and during other cases they exhibit poor performance. Hence, it is proved that the proposed encryption-based technique is the most suitable solution for reconfiguring the PV array.

6. Performance assessment with Non-parametric Wilcoxon signed rank test

To substantiate the effectiveness and consistency of the proposed ACM over the existing reconfiguration techniques statistically, a Non-parametric Wilcoxon Signed-Rank Test [54] with a significant difference of 0.05 has been evaluated. A pairwise unbiased comparative analysis of the proposed technique with others as detailed in Table 5 is executed as follows:

1. Procure the GMP values obtained by all the configurations for different PV array sizes under the considered shading conditions.
2. Evaluate '$R+$', the sum of positive ranks for which the proposed ACM configuration delivers the highest GMP over the existing configurations.
3. Evaluate '$R-$', the sum of negative ranks for which the existing configurations render more GMP compared to the proposed ACM.
4. Evaluate ρ-value that shows the significant difference of the obtained results in a statistical hypothesis testing. The lesser the ρ-value (ρ-value < 0.05), there is much evidence against the null hypothesis

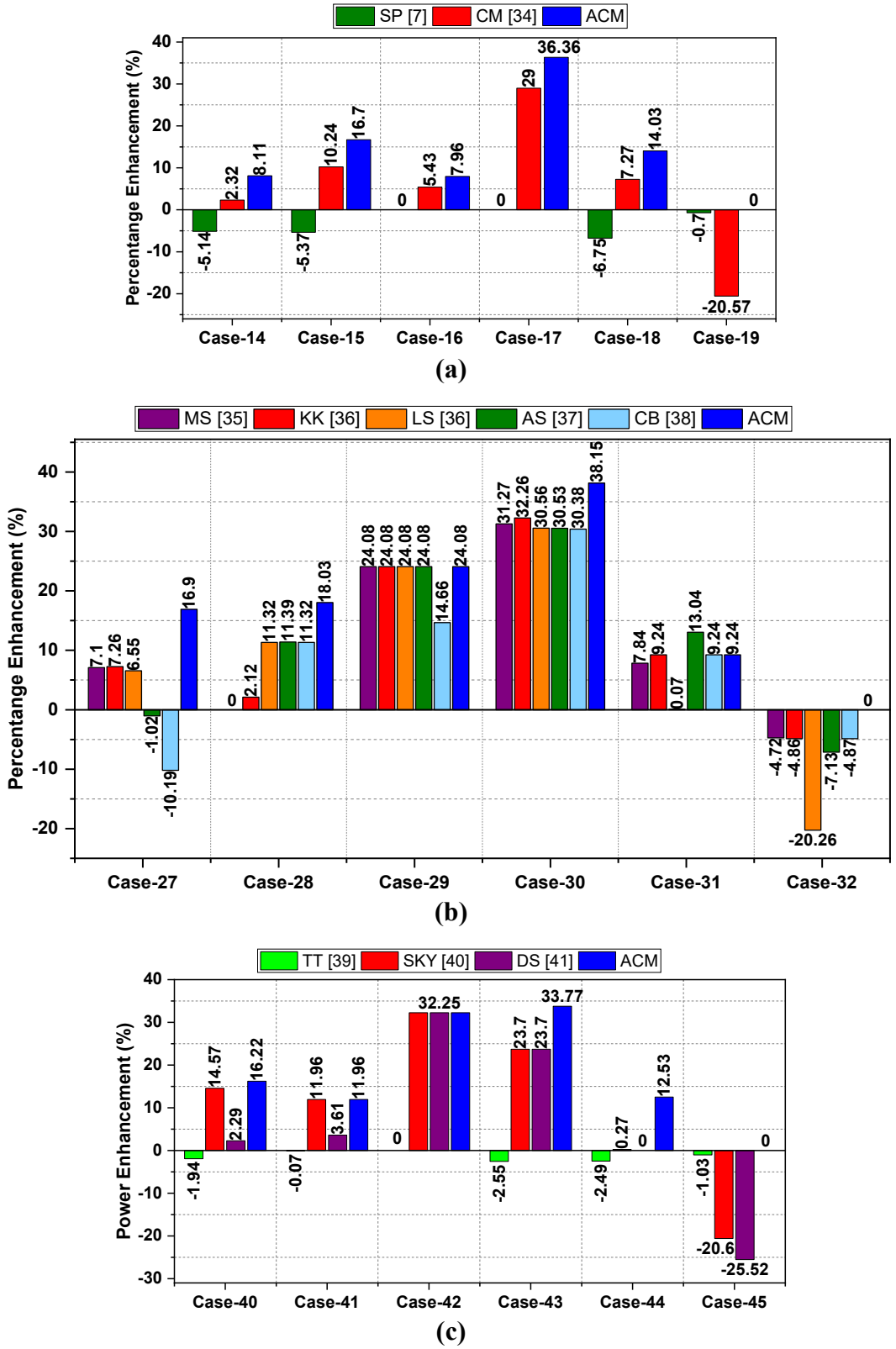

Fig. 30. Power enhancement in various cases for (a) 7 × 7, (b) 6 × 6, (c) 5 × 5, (d) 4 × 4, (e) 4 × 3, (f) 5 × 9, and (g) 6 × 20 PV arrays.

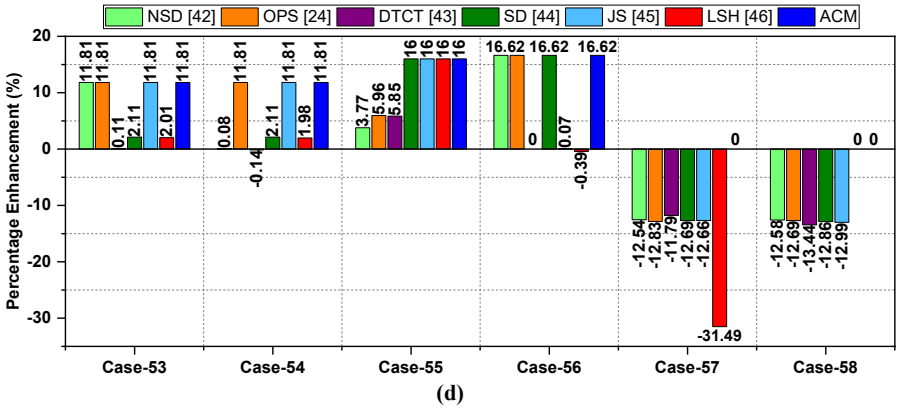

(d)

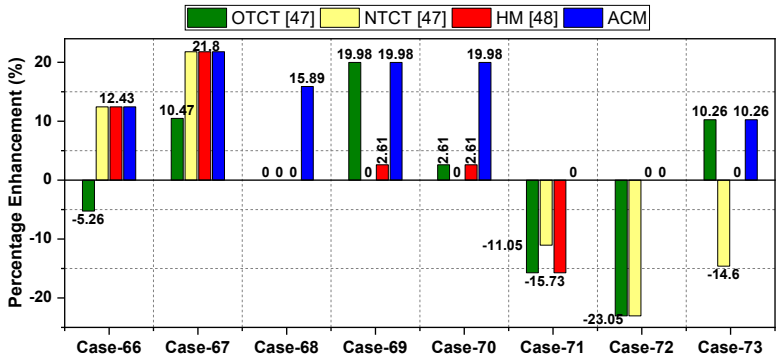

(e)

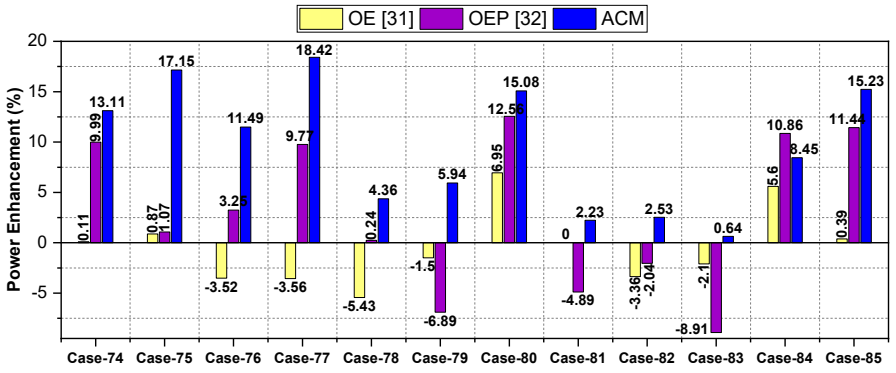

(f)

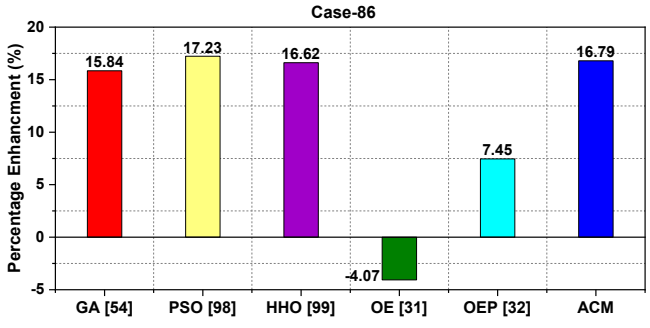

(g)

Fig. 30. (*continued*).

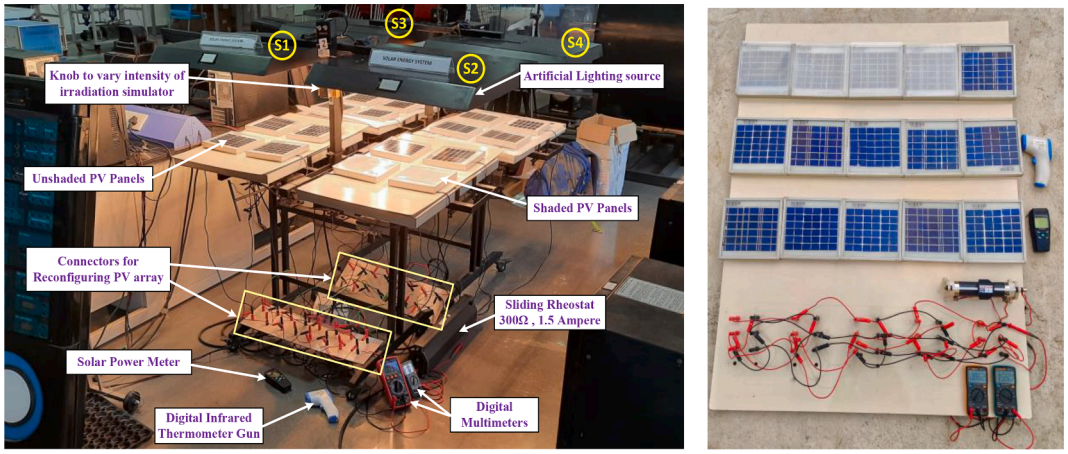

Fig. 31. Experimental prototypes developed and tested in (a) laboratory and (b) outdoor environments for various configurations of 4 × 4 and 3 × 5 PV arrays.

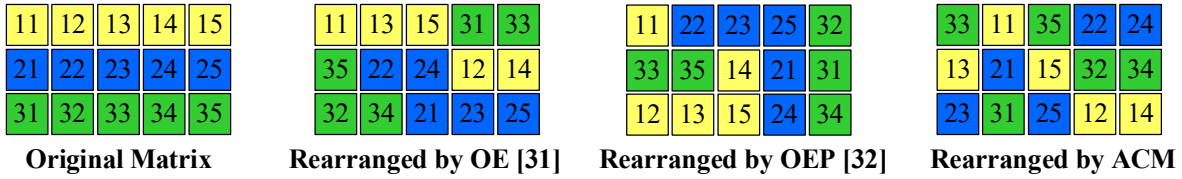

Fig. 32. Original 3 × 5 matrix and the corresponding rearrangement by OE, OEP and ACM techniques.

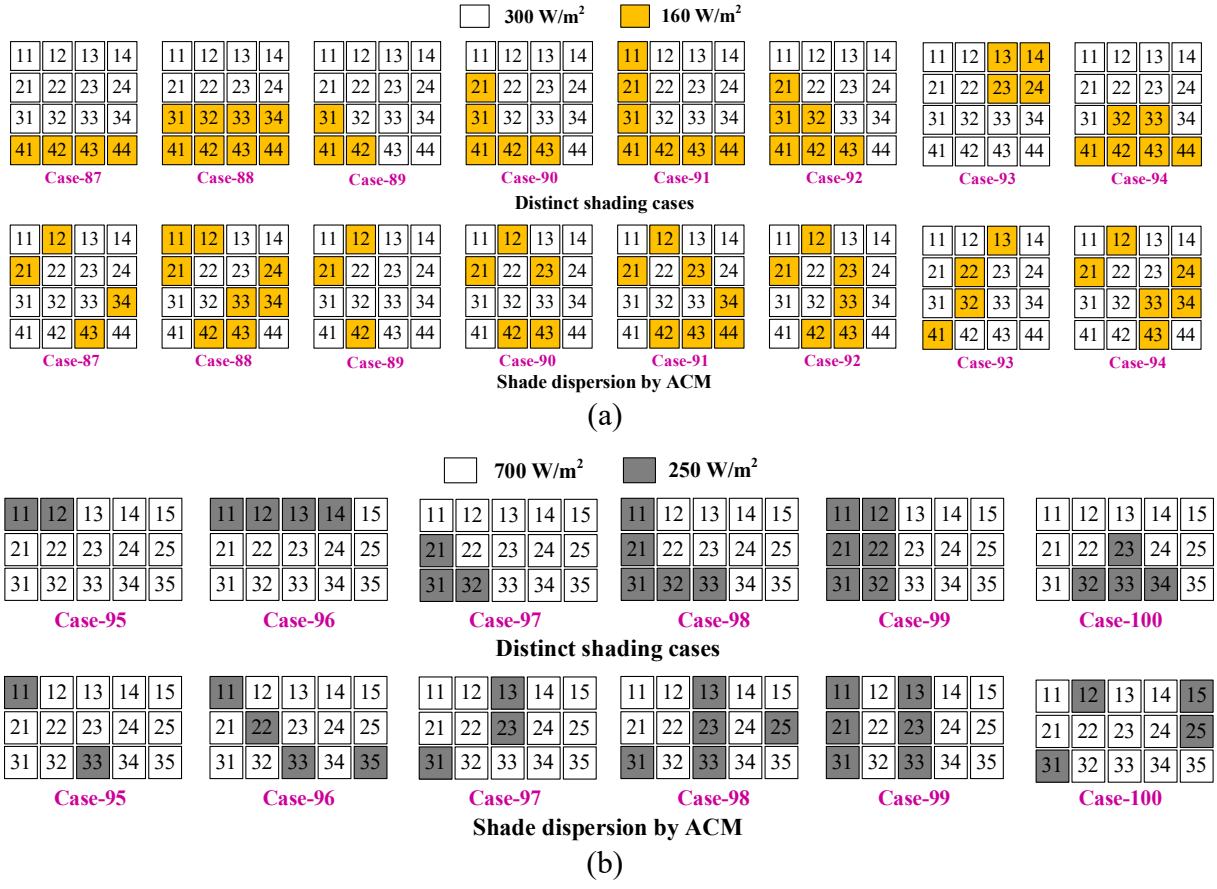

Fig. 33. Distinct shading cases and corresponding shade dispersion by ACM for (a) 4 × 4 and (b) 3 × 5 arrays.

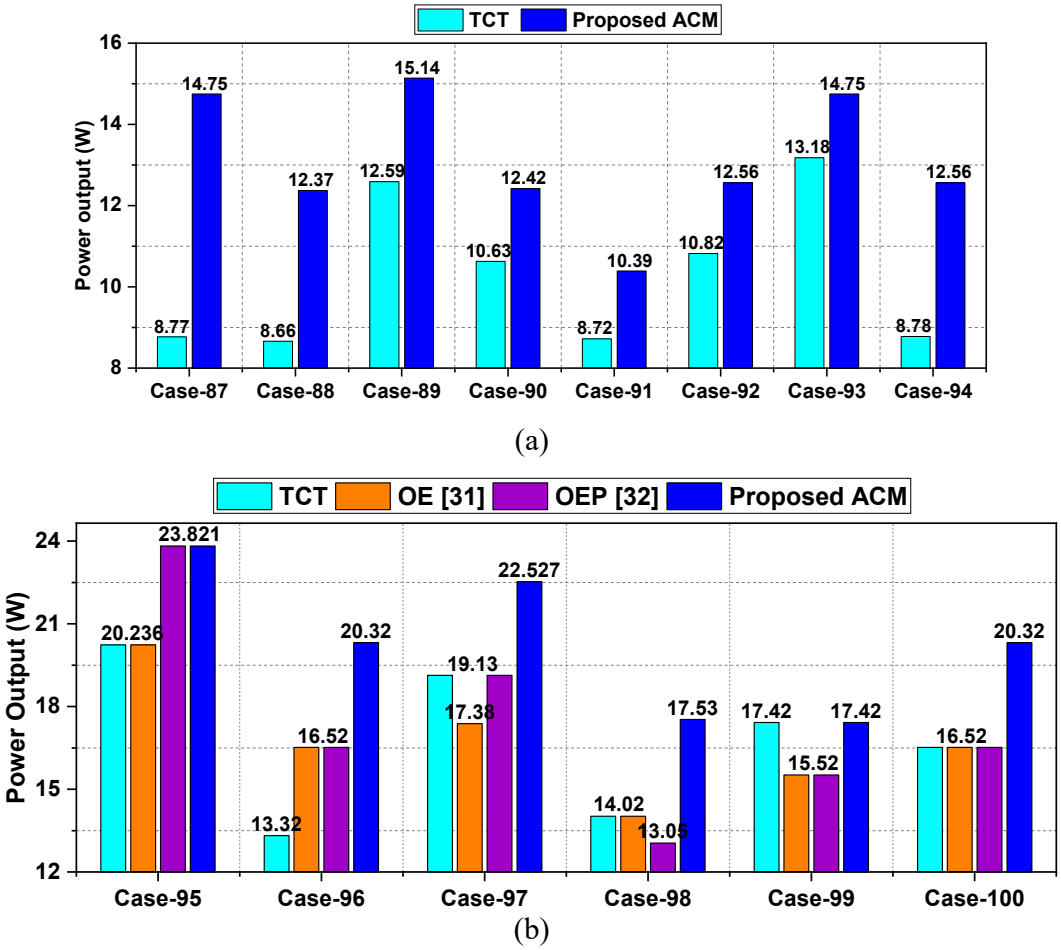

Fig. 34. A comparative experimental results of output power of (a) 4 × 4 and (b) 3 × 5 arrays under various cases.

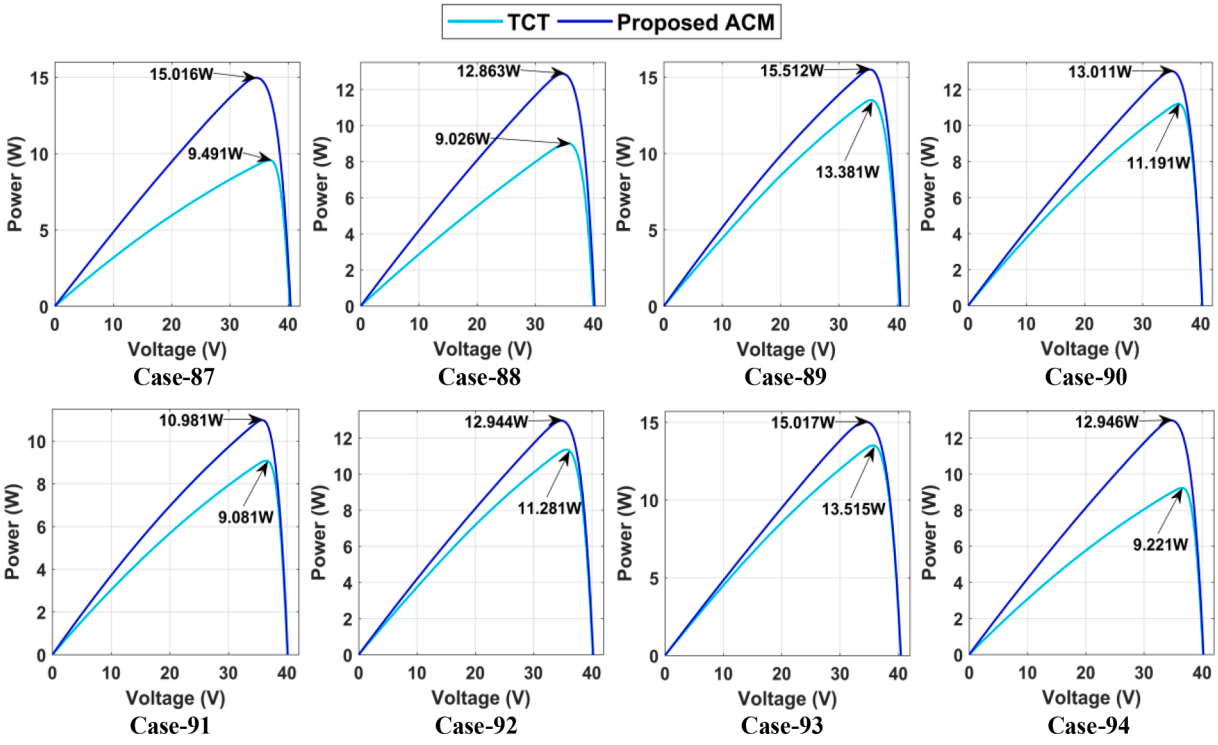

Fig. 35. PV characteristics of a 4 × 4 array under Case-87 to Case-94.

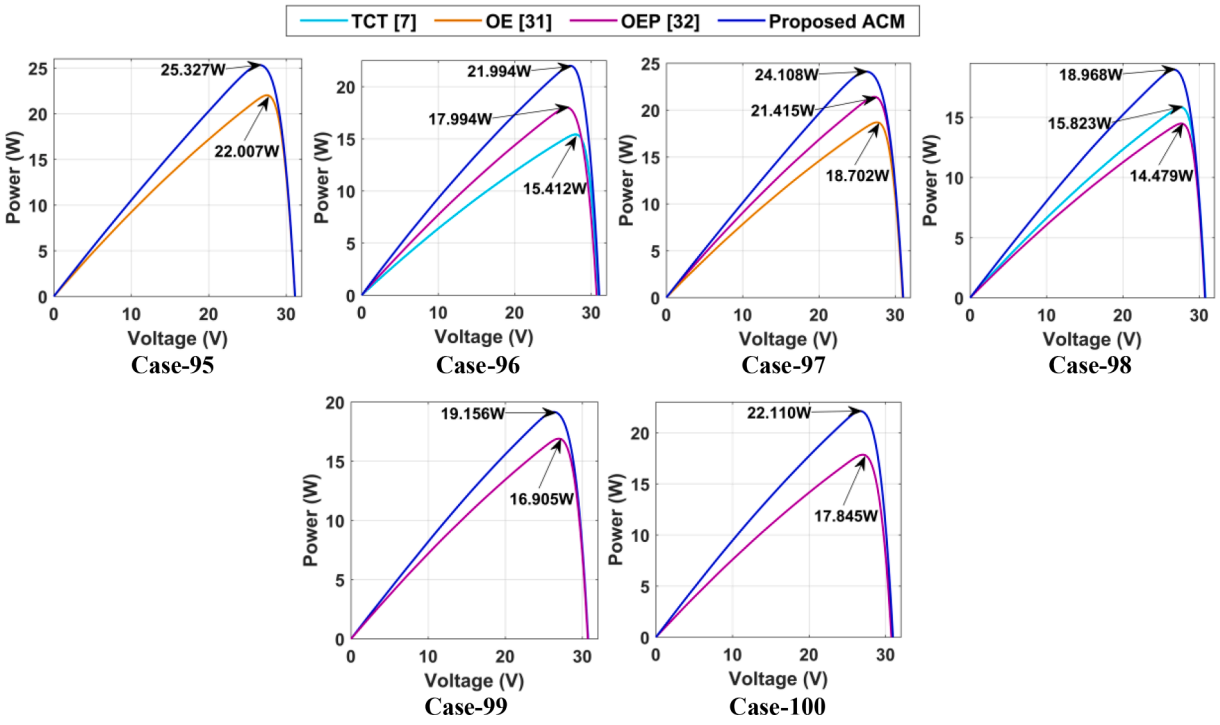

Fig. 36. PV characteristics of a 3 × 5 array under Case-95 to Case-100.

Table 5
A pairwise comparative analysis of all configurations using Non-parametric Wilcoxon signed-rank test.

Array size															
9 × 9								7 × 7					6 × 6		
ACM vs	R_+	R_-	p-value	ACM vs	R_+	R_-	p-value	ACM vs	R_+	R_-	p-value	ACM vs	R_+	R_-	p-value
TCT [7]	15	0	0.0431	**FP** [25]	15	0	0.0431	**SP** [7]	21	0	0.0277	**TCT** [7]	15	0	0.0431
SDK [19]	15	0	0.0431	**OSB** [26]	15	0	0.0431	**TCT** [7]	15	0	0.0431	**MS** [35]	15	0	0.0431
OS [20]	13	**2**	0.138	**SMT** [27]	15	0	0.0431	**CM** [34]	21	0	0.0277	**KK** [36]	10	0	0.0678
IS [21]	15	0	0.0431	**NCI** [28]	15	0	0.0431					**LAS** [36]	15	0	0.0431
ADV [22]	15	0	0.0431	**SKP** [29]	10	0	0.0670					**AS** [37]	14	**1**	0.0796
CS [23]	15	0	0.0431	**LS** [30]	6	0	0.1088					**CB** [38]	15	0	0.0431
MDS [23]	15	0	0.0431	**OE** [31]	15	0	0.0431								
NA [33]	15	0	0.0431	**OEP** [32]	15	0	0.0431								
NOS [24]	15	0	0.0221												

Array size															
5 × 5				4 × 4				4 × 3				3 × 5			
ACM vs	R_+	R_-	p-value	ACM vs	R_+	R_-	p-value	ACM vs	R_+	R_-	p-value	ACM vs	R_+	R_-	p-value
TCT [7]	15	0	0.0431	**TCT** [7]	10	0	0.0679	**TCT** [7]	21	0	0.0277	**TCT** [7]	15	0	0.0431
TT [39]	21	0	0.0277	**OPS** [24]	6	0	0.1080	**OTCT**[47]	21	0	0.0277	**OE** [31]	21	0	0.0277
SKY [40]	10	0	0.0670	**NSD** [42]	10	0	0.0678	**NTCT**[47]	21	0	0.0277	**OEP** [32]	21	0	0.0277
DS [41]	15	0	0.0431	**DTCT** [43]	21	0	0.0277	**HM** [48]	15	0	0.0431		**5 × 9**		
				SD [44]	10	0	0.0678					**TCT** [7]	78	0	0.0022
				JS [45]	6	0	0.1088					**OE** [31]	78	0	0.0022
				LSH [46]	10	0	0.0678					**OEP** [32]	77	1	0.0028

which signifies a notable difference between the effectiveness of configurations.

The results shown in Table 5 confirm that there exists a substantial difference between the proposed ACM and existing configurations as the ρ -values are far lesser than 0.05. The calculated values of $R+$ and $R-$ ascertain that the ACM is competent enough of attaining the highest GMP amongst all where $R+$ is significantly higher than $R-$ for all array sizes. Amongst all configurations, a very few techniques such as OS [20], OPS [24], LS [30], JS [46] exhibit slightly greater ρ-values with respect to the proposed ACM implying that there is no considerable difference in their performance. Even though their performance is slightly on par with ACM, they are not compatible with all PV arrays which is a major drawback. Hence it is concluded that the proposed ACM validates its pre-eminence in rendering a consistently superior performance for various array sizes under all shading conditions. The radar charts depicting the comparative performance analysis of various reconfiguration strategies are shown in Fig. 37.

7. Conclusions

The comprehensive literature of various reconfiguration techniques

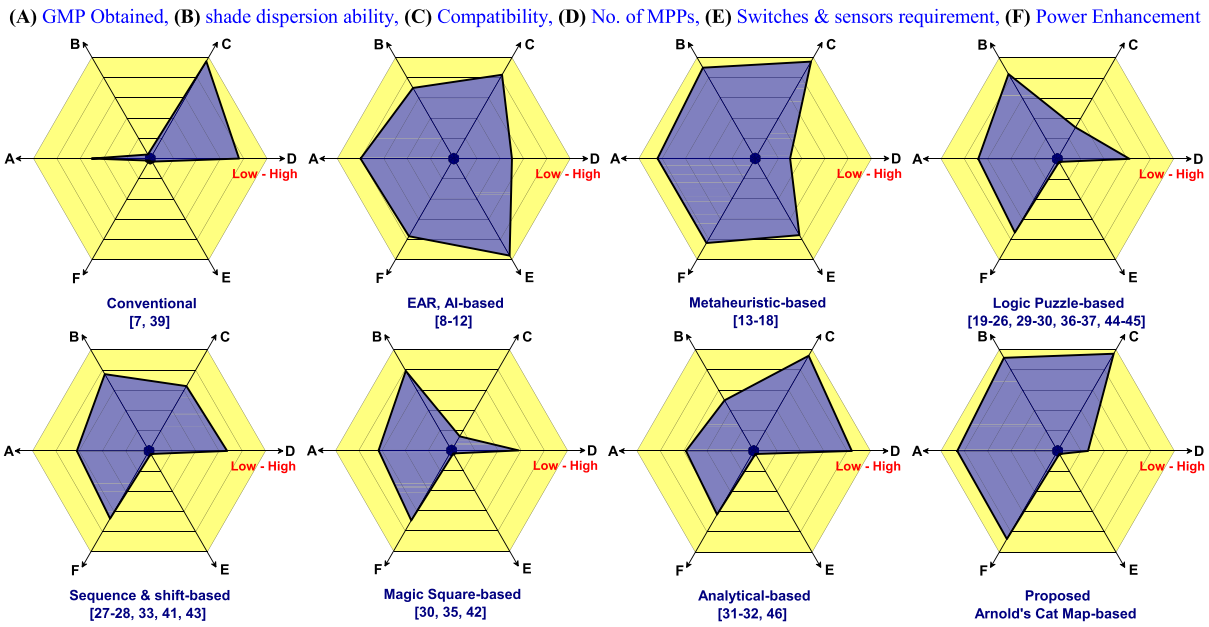

Fig. 37. Radar charts depicting the comparative performance analysis of various reconfiguration strategies.

Appendix

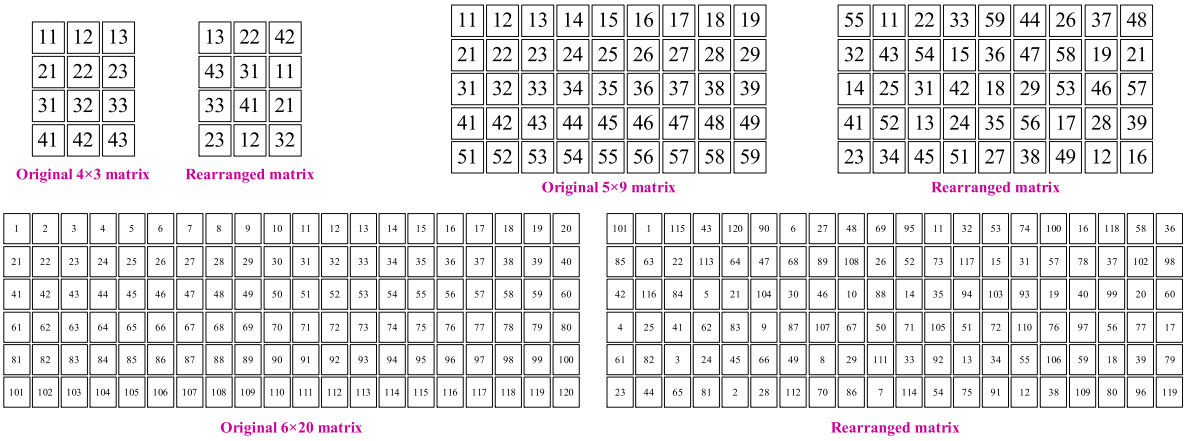

Fig. 38. Original matrices and the corresponding rearrangement by ACM for 4 × 3, 5 × 9, and 6 × 20 PV arrays.

with their advantages and disadvantages is reviewed in detail. A novel reconfiguration technique inspired by the image encryption concept is proposed in this work to reconfigure the PV array optimally to alleviate the shading losses. The proposed technique resolves the setbacks of the existing ones to a greater extent. Further, it is validated for various symmetrical and unsymmetrical PV arrays under 100 shading cases. The effectiveness of the proposed technique is compared with 41 existing and recently reported reconfiguration techniques. Employing ACM, the power enhancement is found to be in the range of (4.96–30.81)%, (7.96–36.36)%, (9.24–38.15)%, (11.96–33.77)%, (11.81–16.62)%, (10.26–21.8)%, (0.64–18.42)%, 16.79% for 9 × 9, 7 × 7, 6 × 6, 5 × 5, 4 × 4, 4 × 3, 5 × 9, 6 × 20 PV arrays respectively. The uniqueness of ACM is its effectiveness in uniformly dispersing the shade by reducing the correlation between the adjacent shaded panels in an array mitigating the mismatch in row currents. This unique feature has led to the highest GMP and smoother array characteristics reducing the MPPs that are highly advantageous for MPPT controllers to track GMP easily. The proposed technique is validated experimentally in both indoor laboratory and outdoor environments. The least p-value of the Non-parametric Wilcoxon Signed-Rank test proves the reliability, effectiveness, and consistency of ACM over the existing ones. It is remarked from the in-depth quantitative and qualitative analysis that the proposed encryption based-technique is proved to be highly effective in mitigating the shading impacts significantly.

8. Data availability statement

Data sharing is not applicable to this article as no new data were created or analyzed in this study.

CRediT authorship contribution statement

Rayappa David Amar Raj: Conceptualization, Methodology, Formal analysis, Writing – original draft, Investigation. **Kanasottu Anil**

Naik: Project administration, Resources, Software, Supervision, Validation, Visualization, Writing – review & editing.

Declaration of Competing Interest

The authors declare that they have no known competing financial interests or personal relationships that could have appeared to influence the work reported in this paper.

References

[1] Mazzeo D, Matera N, Bevilacqua P, Arcuri N. Energy and economic analysis of solar photovoltaic plants located at the university of Calabria. Int J Heat Technol 2015; 33(4):41–50.
[2] Hanser P, Lueken R, Gorman W, Mashal J. The practicality of distributed PV-battery systems to reduce household grid reliance. Utilities Policy 2017;46:22–32.
[3] Herdem MC, Mazzeo D, Matera N, Wen JZ, Nathwani J, Hong Z. Simulation and modeling of a combined biomass gasification-solar photovoltaic hydrogen production system for methanol synthesis via carbon dioxide hydrogenation. Energy Convers Manage 2020;219:113045.
[4] Mirza AF, Mansoor M, Ling Q. A novel MPPT technique based on Henry gas solubility optimization. Energy Convers Manage 2020;225:113409.
[5] Kour J, Shukla A. Enhanced energy harvesting from rooftop PV array using Block Swap algorithm. Energy Convers Manage 2021;247:114691.
[6] Yang B, Ye H, Wang J, Li J, Wu S, Li Y, Shu H, Ren Y. PV arrays reconfiguration for partial shading mitigation: recent advances, challenges and perspectives. Energy Convers Manage 2021;247:114738.
[7] Yadav AS, Mukherjee V. Conventional and advanced PV array configurations to extract maximum power under partial shading conditions: a review. Renewable Energy 2021;178:977–1005.
[8] Sanseverino ER, Ngoc TN, Cardinale M, Vigni VL, Musso D, Romano P, et al. Dynamic programming and Munkres algorithm for optimal photovoltaic arrays reconfiguration. Sol Energy 2015;122:347–58.
[9] Huang Y, Chen X, Ye C. Implementation of a modified circuit reconfiguration strategy in high concentration photovoltaic modules under partial shading. Sol Energy 2019;194:628–48.
[10] Srinivasan A, Devakirubakaran S, Meenakshi Sundaram B. Meenakshi Sundaram, Mitigation of mismatch losses in solar PV system – Two-step reconfiguration approach. Sol Energy 2020;206:640–54.
[11] Karakose M, Baygin M, Murat K, Baygin N, Akin E. Fuzzy based reconfiguration method using intelligent partial shadow detection in PV arrays. Int J Comput Intell Syst 2016;9(2):202–12.
[12] Bouselham L, Rabhi A, Hajji B, Mellit A. Photovoltaic array reconfiguration method based on fuzzy logic and recursive least squares: an experimental validation. Energy 2021;232:121107.
[13] Deshkar SN, Dhale SB, Mukherjee JS, Babu TS, Rajasekar N. Solar PV array reconfiguration under partial shading conditions for maximum power extraction using genetic algorithm. Renew Sustain Energy Rev 2015;43:102–10.
[14] Babu TS, Ram JP, Dragičević T, Miyatake M, Blaabjerg F, Rajasekar N. Particle swarm optimization based solar PV array reconfiguration of the maximum power extraction under partial shading conditions. IEEE Trans Sustainable Energy 2018;9 (1):74–85.
[15] Yousri D, Thanikanti SB, Balasubramanian K, Osama A, Fathy A. Multi-objective grey wolf optimizer for optimal design of switching matrix for shaded PV array dynamic reconfiguration. IEEE Access 2020;8:159931–46.
[16] Yousri D, Allam D, Eteiba MB. Optimal photovoltaic array reconfiguration for alleviating the partial shading influence based on a modified harris hawks optimizer. Energy Convers Manage 2020;206:112470.
[17] Rezk H, Fathy A, Aly M. A robust photovoltaic array reconfiguration strategy based on coyote optimization algorithm for enhancing the extracted power under partial shadow condition. Energy Rep 2021;7:109–24.
[18] Yang B, Shao R, Zhang M, Ye H, Liu B, Bao T, Wang J, Shu H, Ren Y. Socio-inspired democratic political algorithm for optimal PV array reconfiguration to mitigate partial shading. Sustain Energy Technol Assess 2021;48:101627.
[19] Rani BI, Ilango GS, Nagamani C. Enhanced power generation from PV array under partial shading conditions by shade dispersion using Su Do Ku configuration. IEEE Trans Sustainable Energy 2013;4(3):594–601.
[20] Krishna SG, Moger T. Optimal SuDoKu reconfiguration technique for total-cross-tied PV array to increase power output under non-uniform irradiance. IEEE Trans Energy Convers 2019;34(4):1973–84.
[21] Krishna GS, Moger T. Improved SuDoKu reconfiguration technique for total-cross-tied PV array to enhance maximum power under partial shading conditions. Renew Sustain Energy Rev 2019;109:333–48.
[22] Bharti G, Tatabhatla VMR, Kanumuri T. Power Maximization Under Partial Shading Conditions Using Advanced Sudoku Configuration, Proceedings of the International Conf. on Paradigms of Computing, Communication and Data Sciences, Chapter 15, 2021.
[23] Anjum S, Mukherjee V, Mehta G. Advanced SuDoKu-based reconfiguration strategies for maximum power extraction from partially shaded solar photovoltaic array. ASME J Sol Energy Eng 2021;143(6):061003.
[24] Horoufiany M, Ghandehari R. Optimization of the Sudoku based reconfiguration technique for PV arrays power enhancement under mutual shading conditions. Sol Energy 2018;159:1037–46.
[25] Sahu HS, Nayak SK, Mishra S. Maximizing the power generation of a partially shaded PV array. IEEE J Emerg Selected Top Power Electron 2016;4(2):626–37.
[26] Potnuru SR, Pattabiraman D, Ganesan SI, Nagamani C. Positioning of PV panels for reduction in line losses and mismatch losses in PV array. Renewable Energy 2015; 78:264–75.
[27] Belhaouas N, Ait Cheikh M-S, Agathoklis P, Oularbi M-R, Amrouche B, Sedraoui K, et al. PV array power output maximization under partial shading using new shifted PV array arrangements. Appl Energy 2017;187:326–37.
[28] Pillai DS, Ram JP, Nihanth MSS, Rajasekar N. A simple, sensorless and fixed reconfiguration scheme for maximum power enhancement in PV systems. Energy Convers Manage 2018;172:402–17.
[29] Nihanth MSS, Ram JP, Pillai DS, Ghias AMYM, Garg A, Rajasekar N. Enhanced power production in PV arrays using a new skyscraper puzzle based one-time reconfiguration procedure under partial shade conditions (PSCs). Sol Energy 2019; 194:209–24.
[30] Venkateswari R, Rajasekar N. Power enhancement of PV system via physical array reconfiguration based Lo Shu technique. Energy Convers Manage 2020;215: 112885.
[31] Jalil MF, Khatoon S, Nasiruddin I, Bansal RC. An improved feasibility analysis of photovoltaic array configurations and reconfiguration under partial shading conditions. Electr Power Compon Syst 2020;48(9–10):1077–89.
[32] Reddy SS, Yammani C. Odd-Even-Prime pattern for PV array to increase power output under partial shading conditions. Energy 2020;213:118780. ISSN 0360-5442.
[33] Nihanth MSS, Rajasekar N, Pillai DS, Ram JP. A New Array Reconfiguration Scheme for Solar PV Systems Under Partial Shading Conditions. In: Kalam A., Niazi K., Soni A., Siddiqui S., Mundra A. (eds) Intelligent Computing Techniques for Smart Energy Systems. Lecture Notes in Electrical Engineering, vol 607. 2020, Springer, Singapore.
[34] Tatabhatla VMR, Agarwal A, Kanumuri T. A chaos map based reconfiguration of solar array to mitigate the effects of partial shading. IEEE Trans Energy Convers.
[35] Samikannu SM, Namani R, Subramaniam SK. Power enhancement of partially shaded PV arrays through shade dispersion using magic square configuration. J Renewable Sustainable Energy 2016;8:063503.
[36] Yadav AS, Mukherjee V. Line losses reduction techniques in puzzled PV array configuration under different shading conditions. Sol Energy 2018;171:774–83.
[37] Tatabhatla VMR, Agarwal A, Kanumuri T. Performance enhancement by shade dispersion of Solar Photo-Voltaic array under continuous dynamic partial shading conditions. J Cleaner Prod 2019;213:462–79.
[38] Tatabhatla VMR, Agarwal A, Kanumuri T. Improved power generation by dispersing the uniform and non-uniform partial shades in solar photovoltaic array. Energy Convers Manage 2019;197:111825.
[39] Ramesh T, Rajani K, Panda AK. A novel triple-tied-cross-linked PV array configuration with reduced number of cross-ties to extract maximum power under partial shading conditions. CSEE J Power Energy Syst 2021;7(3):567–81.
[40] Meerimatha G, Rao BL. Novel reconfiguration approach to reduce line losses of the photovoltaic array under various shading conditions. Energy 2020;196:117120.
[41] Dhanalakshmi B, Rajasekar N. Dominance square based array reconfiguration scheme for power loss reduction in solar PhotoVoltaic (PV) systems. Energy Convers Manag 2018;156:84–102.
[42] Rakesh N, Madhavaram TV. Performance enhancement of partially shaded solar PV array using novel shade dispersion technique. Front Energy 2016;10(2):227–39.
[43] Madhanmohan VP, Nandakumar M, Saleem A. Enhanced performance of partially shaded photovoltaic arrays using diagonally dispersed total cross tied configuration. Energy Sourc, Part A: Recov Util Environ Effects 2020.
[44] Srinivasan S, Devakirubakaran B, Sundaram M. Mitigation of mismatch losses in solar PV system – Two-step reconfiguration approach. Sol Energy 2020;206: 640–54.
[45] Palpandian M, David PW, Elavarasan RM, Periyasamy P, Pugazhendhi R, Shafiullah GM, Natarajan SK. A Jigsaw Puzzle based Reconfiguration Technique for Enhancing Maximum Power in Partial Shaded Hybrid Photovoltaic Array, 2021.
[46] Srinivasan S, Devakirubakaran B, Sundaram M, Balachandran PK, Cherukuri SN, Winston DP, et al. L-shape propagated array configuration with dynamic reconfiguration algorithm for enhancing energy conversion rate of partial shaded photovoltaic systems. IEEE Access 2021;9:97661–74.
[47] Vijayalekshmy S, Bindu GR, Rama Iyer S. A novel Zig-Zag scheme for power enhancement of partially shaded solar arrays. Sol Energy 2016;135:92–102.
[48] Raj RDA, Naik KA. A generalized henon map-based solar PV array reconfiguration technique for power augmentation and mismatch mitigation. IETE J Res 2022. https://doi.org/10.1080/03772063.2022.2055660.
[49] Zhang X, Li C, Li Z, Yin X, Yang Bo, Gan L, et al. Optimal mileage-based PV array reconfiguration using swarm reinforcement learning. Energy Convers Manage 2021;232:113892.
[50] Wang S, Peng Q, Du B. Chaotic color image encryption based on 4D chaotic maps and DNA sequence. Opt Laser Technol 2022;148:107753.
[51] Carlos Eduardo de Souza, Chaves D, Pimentel C. One-Dimensional Pseudo-Chaotic Sequences Based on the Discrete Arnold's Cat Map Over $\mathbb{Z}_3{}^m$, IEEE Transactions on Circuits and Systems II: Express Briefs, 2021, PP. 1-1. 10.1109/TCSII.2020.3010477.
[52] Abuturab MR. Generalized Arnold map-based optical multiple color-image encoding in gyrator transform domain. Opt Commun 2015;343:157–71.
[53] Koppanati RK, Kumar K. P-MEC: polynomial congruence-based multimedia encryption technique over cloud. IEEE Consum Electron Mag 2021;10(5):41–6.
[54] Harris T, Hardin JW. Exact Wilcoxon Signed-Rank and Wilcoxon Mann-Whitney Ranksum tests. Stata J 2013;13(2):337–43.